

# Asymmetric Activation of the Calcium Sensing Receptor Homodimer

Yang Gao<sup>1,2</sup>, Michael J. Robertson<sup>1,2</sup>, Sabrina N. Rahman<sup>4</sup>, Alpay B. Seven<sup>1,2</sup>, Chensong Zhang<sup>1,2</sup>, Justin G. Meyerowitz<sup>1,2,3</sup>, Ouliana Panova<sup>1,2</sup>, Fadil M. Hannan<sup>5,6</sup>, Rajesh V. Thakker<sup>5</sup>, Hans Bräuner-Osborne<sup>4</sup>, Jesper M. Mathiesen<sup>4,7</sup> & Georgios Skiniotis<sup>1,2,7</sup>

## Affiliations:

<sup>1</sup>Department of Molecular and Cellular Physiology, Stanford University School of Medicine, Stanford, CA 94305, USA.

<sup>2</sup>Department of Structural Biology, Stanford University School of Medicine, Stanford, CA 94305, USA.

<sup>3</sup>Department of Anesthesiology, Perioperative and Pain Medicine, Stanford University School of Medicine, Stanford, CA 94305, USA.

<sup>4</sup>Department of Drug Design and Pharmacology, Faculty of Health and Medical Sciences, University of Copenhagen, Denmark.

<sup>5</sup>Academic Endocrine Unit, Radcliffe Department of Medicine, University of Oxford, Oxford, UK.

<sup>6</sup>Nuffield Department of Women's & Reproductive Health, University of Oxford, Oxford, UK.

<sup>7</sup>Correspondence: jmm@sund.ku.dk or yiorgo@stanford.edu

## Summary

1 The calcium-sensing receptor (CaSR), a cell surface sensor for  $\text{Ca}^{2+}$ , is the master regulator of  
2 calcium homeostasis in humans and is targeted by calcimimetic drugs for the treatment of  
3 parathyroid disorders<sup>1</sup>. CaSR is a family C G protein-coupled receptor (GPCR)<sup>2</sup> that functions as  
4 an obligate homodimer with each protomer comprised of a  $\text{Ca}^{2+}$ -binding extracellular domain  
5 (ECD) and a seven-transmembrane-helix domain (7TM) that activates heterotrimeric G proteins.  
6 Here we show cryo-electron microscopy (cryo-EM) structures of near full-length human CaSR in  
7 inactive or active states bound to  $\text{Ca}^{2+}$  and various calcilytic or calcimimetic drug molecules. We  
8 show that upon activation, the CaSR homodimer adopts an asymmetric 7TM configuration that  
9 primes one protomer for G protein-coupling. This asymmetry is stabilized by 7TM-targeting  
10 calcimimetic drugs adopting distinctly different poses in the two protomers, whereas the binding  
11 of a calcilytic locks CaSR 7TMs in an inactive symmetric configuration. These results provide a

1 detailed structural framework for CaSR activation and the rational design of therapeutics targeting  
2 this receptor.

## Introduction

3 CaSR regulates calcium homeostasis primarily through its actions in the parathyroid gland and  
4 kidneys, where its activation by elevated circulating  $\text{Ca}^{2+}$  leads to decreases in parathyroid  
5 hormone (PTH) secretion and renal tubular  $\text{Ca}^{2+}$  resorption, respectively<sup>1</sup>. CaSR is positively  
6 modulated by various extracellular ligands, including aromatic amino acids, and has thus been  
7 proposed to double as a nutrient sensor<sup>3</sup>. Loss-of-function mutations of CaSR lead to familial  
8 hypocalciuric hypercalcemia type 1 (FHH1), whereas gain-of-function CaSR mutations give rise  
9 to autosomal dominant hypocalcemia type 1 (ADH1)<sup>1</sup>. Moreover, chronic kidney disease (CKD)  
10 frequently reduces parathyroid CaSR expression and function, resulting in secondary  
11 hyperparathyroidism (sHPT)<sup>4</sup>. Currently, CaSR is clinically targeted by three calcimimetic  
12 positive allosteric modulators (PAMs), namely cinacalcet, evocalcet and etelcalcetide, for the  
13 treatment of sHPT and FHH1, while calcilytic negative allosteric modulators (NAMs) are currently  
14 in Phase II clinical trials for the treatment of ADH1<sup>5</sup>.

15 CaSR is a member of family C GPCRs<sup>2</sup>, which also include the metabotropic glutamate receptors  
16 (mGlu). CaSR functions as an obligate homodimer with an N-terminal extracellular domain  
17 (ECD) comprised of a ‘Venus fly trap’ domain (VFT), a bi-lobed (LB1-LB2) structure responsible  
18 for ligand binding, linked to the 7-transmembrane domain (7TM) by a cysteine-rich domain  
19 (CRD). Previous crystal structures of the CaSR ECD<sup>6,7</sup> have illustrated how the binding of  $\text{Ca}^{2+}$   
20 and tryptophan (L-Trp) or its derivatives leads to the closure and reorientation of the VFTs.  
21 However, how ECD rearrangements result in the activation of the 7TMs and how NAMs and  
22 PAMs target the receptor remain unknown. To address these questions, we purified near full-length

human CaSR in active or inactive states (Extended Data Fig. 1a-f) and analyzed these preparations by cryo-EM (Extended Data Figs. 2-4). Here we show two structures of active-state CaSR in complex with clinically used PAMs, namely the CaSR-cinacalcet complex and the CaSR-evocalcet-etelcalcetide complex, at nominal global resolutions of 2.5Å and 2.8Å respectively, together with structures of CaSR complexed with the NAM NPS-2143 under inactive (low Ca<sup>2+</sup>) and activating (high Ca<sup>2+</sup>, high L-Trp) conditions at 4.1Å and 3.2Å respectively (Fig. 1a, Extended Data Figs. 1g,1h,2-4). The results reveal how calcilytic and calcimimetic drugs target CaSR and illustrate an essential asymmetry between the two active-state CaSR protomers stabilized by the same 7TM PAM in two distinct binding poses.

## **Structural rearrangement of CaSR ECD upon activation**

In the inactive state, the CaSR homodimer adopts an extended parallel conformation with an interface involving the upper lobe of the VFTs (LB1), similar to the apo-state mGlu5 homodimer<sup>8</sup> (Extended Data Figs. 1g,5a,b). Notably, the VFTs in the inactive-state cryo-EM structure adopt an asymmetric open-closed conformation, unlike the symmetric open-open inactive ECD crystal structure<sup>6</sup> (Extended Data Figs. 1g,i,5a,c,d). The 7TMs are separated with the TM5-TM6 plane facing each other (Fig. 1b), distinct from the TM4-TM5 interface observed in mGlu5 (Extended Data Fig. 5e)<sup>8</sup>. Upon activation, the closure of VFTs brings the CRDs together (Fig. 1c, Extended Data Fig. 5f), thereby clamping the 7TMs to form a TM6-TM6 interface (Fig. 1b). The juxtaposed TM6 helices diverge from each other on the cytoplasmic side (Fig. 2a), creating a space that accommodates several ordered elongated densities that correspond to cholesterol hemisuccinate (CHS) or GDN detergent, potentially stabilized by a cholesterol-binding CARC motif<sup>9</sup> (805-KFITFSML-812) centered around F809<sup>6,47</sup> (superscript denoting generic GPCR numbering<sup>10</sup>)

(Extended Data Fig. 5g,h). Notably, CaSR has been shown in parathyroid cells to localize to cholesterol-rich caveolae<sup>11</sup>, and F809<sup>6,47</sup>L is an inactivating mutation causing FHH1<sup>12</sup>. The activated ECD adopts a symmetric closed-closed conformation (Fig. 1a,c) with an L-tryptophan (L-Trp) bound at each LB1-LB2 cleft. In each protomer, we observe densities at the four Ca<sup>2+</sup> sites reported in a previous active-state ECD crystal structure<sup>6</sup>, however only two sites contain coordination spheres that support the presence of Ca<sup>2+</sup> (Extended Data Fig. 5i). In the inactive open-closed ECD, the closed protomer (RMSD=0.7Å, Extended Data Fig. 5j) is occupied by a tube-shaped density at the L-Trp site, as in the active state (Extended Data Fig. 5k). A previous crystal structure of the active CaSR ECD without added L-Trp also revealed a density at the LB1-LB2 cleft<sup>7</sup>, that was identified through mass spectroscopy as an L-Trp derivative and proposed to arise from recombinant protein production. Thus, the corresponding density observed in our inactive CaSR map could be of a similar origin. Notably, an open-closed conformation has been observed in crystal structures of mGlu1 ECD (Extended Data Fig. 5l)<sup>13</sup>, where L-Glu also occupies the LB1-LB2 cleft. L-amino acids function as PAMs for CaSR, and the open-closed conformation could be more relevant in nutrient-rich environments, such as the gastrointestinal tract, where amino acid concentrations can increase up to 30 mM after food intake<sup>14</sup>. The binding of L-amino acids or derivatives in one VFT cleft of inactive CaSR may prime the receptor for activation, increasing its sensitivity to fast fluctuations of Ca<sup>2+</sup> concentration.

### **Binding mode of the ECD PAM etelcalcetide**

Etelcalcetide, a newly approved calcimimetic PAM that engages the CaSR ECD<sup>15</sup>, is a 7-residue D-peptide with an N-terminal <sub>D</sub>Cys1 protected by a disulfide-bonded L-cysteine (Fig. 1d). It has been proposed that upon binding this PAM exchanges out the L-cysteine to form a disulfide with CaSR C482<sup>16</sup>. Our 2.5 Å structure of active-state CaSR in complex with both etelcalcetide and the

7TM PAM evocalcet reveals two identical copies of etelcalcetide covalently-bound to C482 of each protomer (Fig. 1c,d and Extended Data Fig. 6a). The binding sites, located at the LB2 interface, are highly enriched in negatively charged residues (Fig. 1c,d). Residues <sub>D</sub>Arg3-4 and <sub>D</sub>Arg5 in etelcalcetide reach out in opposite directions to form salt bridges with a patch of negatively charged residues on the juxtaposed VFTs, while <sub>D</sub>Arg7 extends downward to simultaneously interact with E228 and E241 from opposite protomers. This would stabilize the active closed-closed ECD conformation, providing a molecular mechanism for etelcalcetide PAM activity. Interestingly, <sub>D</sub>Ala2 and <sub>D</sub>Ala6 each point to a different acidic patch on one protomer and the N-terminal acetyl group faces D248 and E251 from the other protomer. These observations suggest that introduction of basic side chains at <sub>D</sub>Ala2 and <sub>D</sub>Ala6 and addition of an N-terminal basic residue could potentially enhance the potency of etelcalcetide.

## **7TM asymmetry in active-state CaSR**

In contrast to the symmetric ECD, the active-state 7TMs adopt significantly asymmetric conformations. Strikingly, this asymmetry is also reflected by the same 7TM PAM assuming distinct poses in the two protomers (Fig. 2a,b, Extended Data Fig. 6b-d). In both active CaSR structures, 7TM<sup>A</sup> contains an extended PAM, while the same PAM in 7TM<sup>B</sup> adopts a bent conformation (Fig. 2a,b, Extended Data Fig. 6c,d). At the 7TM interface, TM6 of 7TM<sup>A</sup> sits higher than the opposing TM6 of 7TM<sup>B</sup> that is tilted relative to 7TM<sup>A</sup> (Fig. 2a,b, Extended Data Fig. 6b). The asymmetric 7TMs are further stabilized by a series of interactions across CRD-ECL2-ECL3 (Fig. 2c, Extended Data Fig. 7a). K601 and W590 of CRD form polar or  $\pi$ - $\pi$  interactions with the D758 main-chain amide at the apex of ECL2. R752 and Q754 of ECL2 are positioned to interact with CRD residues D587 and D588. Notably, R752C, which would weaken CRD-ECL2 interactions, is an inactivating FHH1 mutation<sup>17</sup>. ECL2-ECL3 interactions differ between the two

1 protomers (Fig. 2c). In 7TM<sup>A</sup>, Y829 of ECL3 extends upward to interact with L756 and E757 of  
2 ECL2. This upward ECL3 conformation is further stabilized by the polar interaction between K831  
3 of ECL3 and E610 on top of TM1. In 7TM<sup>B</sup>, ECL3 extends towards the 7TM core with Y829  
4 stabilized by  $\pi$ - $\pi$  interaction with Y825<sup>6,57</sup>. Thus, in active CaSR, the same set of residues form  
5 distinct interaction networks between the two protomers stabilizing different ECL3 conformations.

## 6 **7TM PAMs adopt distinct poses in active CaSR homodimer**

7 Cinacalcet and evocalcet have similar efficacy and potency towards CaSR and share a backbone  
8 architecture with a flexible linker connecting naphthylethylamine and phenyl groups (Fig. 3a,  
9 Extended Data Figs. 1c,d,7b). The linker in cinacalcet is a 3-carbon chain, whereas in evocalcet it  
10 is a pyrrolidine ring adopting alternative *endo* or *exo* envelope conformers. In both the extended  
11 and bent conformations, which were evaluated and optimized using GemSpot<sup>18</sup> (Fig. 3a, Extended  
12 Data Fig. 7c), the naphthylethylamine group assumes highly similar positions, with the secondary  
13 amine stabilized by polar interactions with Q681<sup>3,33</sup> and E837<sup>7,32</sup>. The naphthyl group forms  
14 hydrophobic interactions with F684<sup>3,36</sup> and I777<sup>5,44</sup> on one side and edge-to-face  $\pi$ - $\pi$  interactions  
15 with W818<sup>6,50</sup> on the other, holding the W818<sup>6,50</sup> sidechain inside the 7TM core. In the extended  
16 PAM, the linker together with the phenyl group extend upwards parallel to TM6 pushing Y825<sup>6,57</sup>  
17 to point downward. In the bent PAM, the phenyl group folds down toward the gap between TM5  
18 and TM6, forming parallel-displaced  $\pi$ - $\pi$  stacking with the naphthyl group, while Y825<sup>6,57</sup> adopts  
19 a near-horizontal conformation to stabilize the bent linker through  $\sigma$ - $\pi$  interaction. In agreement  
20 with the observed PAM binding modes, the mutation Q681<sup>3,33</sup>A substantially attenuated  
21 cinacalcet-enhancement of CaSR signaling in inositol monophosphate (IP<sub>1</sub>) accumulation assays  
22 (Extended Data Fig. 8a). Furthermore, E837<sup>7,32</sup>A, F684<sup>3,36</sup>A and W818<sup>6,50</sup>A have been shown to  
23 significantly weaken cinacalcet-induced potentiation for CaSR<sup>19</sup>.

## **The 7TM with an extended PAM favors G protein activation**

Family C GPCR dimers have been proposed to engage one G protein at a time<sup>20,21</sup>. The observed active-state CaSR asymmetry suggests that one protomer is primed to couple to G protein, in agreement with our active mGlu2 structures alone and complexed with G<sub>i</sub> (companion manuscript). To determine which CaSR 7TM is primed for G protein-coupling we utilized the quality control system of heterodimeric GABA<sub>B</sub> receptors<sup>22</sup> to display a CaSR heterodimer at the plasma membrane (Fig. 3b, Extended Data Fig. 8b). The C-terminal coiled-coil domain of either GABA<sub>B1</sub> or GABA<sub>B2</sub> together with an ER retention sequence KKTN were fused to the C-terminus of CaSR, resulting in CaSR-C1 and CaSR-C2 constructs. Cell surface ELISA assays verified that only a CaSR heterodimer can reach the cell surface with equivalent expression and membrane localization levels amongst different constructs (Extended Data Fig. 8b). Aiming to directly probe the effects of PAM binding perturbations in G<sub>q</sub> signaling at the CaSR-C1 protomer, we introduced E837<sup>7.38</sup>A and F801<sup>ICL3</sup>A that block PAM-binding<sup>19</sup> and G protein-coupling<sup>21</sup> at the CaSR-C2 protomer (Fig. 3b). We then introduced mutations to CaSR-C1, sterically occluding either bent (C781<sup>5.48</sup>W, I822<sup>6.54</sup>W, favoring extended) or extended (L773<sup>5.40</sup>W, V833<sup>7.28</sup>W, favoring bent) PAM conformations (Fig. 3a,b, Extended Data Fig. 8c). Both mutant heterodimers responded to Ca<sup>2+</sup> similarly to the wild-type, verifying the functionality of the mutants (Fig. 3b). In the presence of cinacalcet the wild-type construct displayed an expected increase in E<sub>max</sub> and leftward shift of the Ca<sup>2+</sup> response curve. In contrast, the mutant favoring the bent PAM conformation showed a substantially blunted PAM enhancement, while the mutant favoring the extended PAM displayed an increase in PAM enhancement compared to wild-type (Fig. 3b). These results suggest that 7TM<sup>A</sup> with extended PAM is favored in G protein-coupling. Of note, TM6 of 7TM<sup>A</sup> is positioned higher than the juxtaposed TM6 of 7TM<sup>B</sup> (Fig. 2b,c, Extended Data Fig. 7a) in a fashion analogous

1 to the TM6 configuration in both active-state and G protein-coupling mGlu2 structures  
2 (companion manuscript, Extended Data Fig. 9b,c).

3 Difference in G protein-coupling propensities of 7TM<sup>A</sup> and 7TM<sup>B</sup> is also supported by  
4 observations related to CaSR C-termini. Although disordered in 7TM<sup>A</sup>, an ordered C-terminus  
5 encompassing residues 877-888 in 7TM<sup>B</sup> is observed sequestered in detergent micelle (Fig. 2a,  
6 Extended Data Fig. 9a). Previous studies have shown this region to be essential for CaSR signaling  
7 through G<sub>q</sub><sup>23</sup>. Furthermore, our mGlu2-Gi complex structure illustrates the critical role of the C-  
8 terminus in G protein-coupling. Notably, superposition of the mGlu2 G protein-coupling 7TM  
9 onto CaSR 7TM<sup>A</sup> with extended PAM shows that they adopt similar conformations, with the G  
10 protein well accommodated on a membrane plane (Extended Data Fig. 9c). The 7TM asymmetry  
11 in CaSR is more pronounced than mGlu2, with 7TM<sup>B</sup> tilting further to sequester its C-terminus on  
12 the membrane, likely precluding G protein-coupling on 7TM<sup>B</sup>.

### 13 **NAM binding in symmetric CaSR 7TMs**

14 The inactive-state CaSR is highly flexible, limiting the overall achievable resolution of our  
15 structure to 4.1 Å, with local 7TMs and ECDs refinements reaching 3.9 Å and 3.7 Å respectively  
16 (Extended Data Fig. 4a-b). Inactive-state CaSR displays symmetric 7TMs where we observe clear  
17 densities for the NAM NPS-2143, and surrounding residues (Extended Data Figs. 1g,4a,6g-h). In  
18 order to understand NAM inhibition under activating conditions, we purified CaSR in the presence  
19 of NPS-2143 with high concentrations of Ca<sup>2+</sup> and L-Trp (CaSR-NAM-Ca<sup>2+</sup>-Trp) and obtained its  
20 cryo-EM structure (Extended Data Figs. 1h,4c-d). The ECD of CaSR-NAM-Ca<sup>2+</sup>-Trp is identical  
21 to the active-state (RMSD=0.3Å), and the higher rigidity allowed us to achieve 3.2 Å global  
22 resolution. The conformation of the NAM-bound 7TMs agrees well with the inactive-state  
23 structure (Fig. 3c, Extended Data Fig. 6e,g,h). Notably, unlike the asymmetric 7TMs configuration



observed in the active-state, the NAM-bound 7TMs are fully symmetric (Fig. 4a, Extended Data Fig. 6f) and the 7TM interface is distinct from the asymmetric interface observed in active-state CaSR (Fig. 4b, Extended Data Fig. 6b,f). When one 7TM of CaSR-NAM-Ca<sup>2+</sup>-Trp is aligned onto the active-state 7TM<sup>B</sup>, the other 7TM is positioned away from 7TM<sup>A</sup> (Fig. 4b). The NAM NPS-2143 shares a similar molecular architecture with the phenylalkylamine PAMs and binds through comparable polar interactions with Q681<sup>3.33</sup> and E837<sup>7.32</sup> (Fig. 3c). In our IP<sub>1</sub> accumulation assays, Q681<sup>3.33</sup>A substantially attenuated CaSR inhibition by NPS-2143 (Extended Data Fig. 8a) while E837<sup>7.32</sup>A has previously been shown to blunt the NAM effect of NPS-2143<sup>19</sup>. However, there are two significant differences between the NAM and PAM (Fig. 3a,c). The longer linker between the secondary amine and the benzonitrile group allows the NAM to interact with F821<sup>6.53</sup> and Y825<sup>6.57</sup>, while the addition of a quaternary carbon angles the naphthyl group towards a hydrophobic TM6-TM7 cleft forming  $\pi$ - $\pi$  interactions with F821<sup>6.53</sup> and F814<sup>6.46</sup>, thereby locking W818<sup>6.50</sup> in an outward-facing conformation (Fig. 3c). These interactions likely rigidify the top of TM6, preventing the formation of the staggered active-state asymmetric interface.

### **Distinct mechanism of the family C GPCR toggle switch**

The most notable differences between inactive and active-state CaSR 7TMs lie in TM6 (Figs. 3a,c,4c). Upon activation, TM6 forms a kink at P823<sup>6.55</sup> and the cytoplasmic half of the helix rotates inward as evident in the F821<sup>6.53</sup> and W818<sup>6.50</sup> conformations. F821<sup>6.53</sup> inserts into a TM6-TM7 hydrophobic cleft, while W818<sup>6.50</sup> is pushed inward by  $\pi$ - $\pi$  interactions with PAMs. By contrast, in the inactive-state, TM6 forms a continuous  $\alpha$ -helix. NAM pushes W818<sup>6.50</sup> to face outward while stabilizing F821<sup>6.53</sup> toward TM5. P823<sup>6.55</sup>A, which would hinder TM6-kink formation, has been shown to ablate Ca<sup>2+</sup> response by CaSR<sup>24</sup>, whereas A824<sup>6.56</sup>P and F821<sup>6.53</sup>L, which would, respectively, facilitate TM6-kink formation and ease the inward rotation of TM6,

are activating ADH mutations<sup>17,25</sup>. Furthermore, F821<sup>6.53</sup>A has been shown to impair NAM inhibition while enhancing PAM potentiation<sup>19</sup>. These observations point to the importance of the TM6 region surrounding W818<sup>6.50</sup> in CaSR activation and modulator-binding. The W<sup>6.50</sup> residue is highly conserved in family C GPCRs, forming a TM6 toggle switch motif (WxxFxP) reminiscent to the CWxP<sup>6.50</sup> motif surrounding W<sup>6.48</sup> toggle switch in family A GPCRs<sup>26</sup> (Fig. 4e). The family A toggle switch W<sup>6.48</sup> is displaced to drive the opening of TM6 at the cytoplasmic end (Fig. 4d). However, the CaSR toggle switch W<sup>6.50</sup> moves in a distinct direction, transiting from outward-facing to inward-facing upon activation (Fig. 4c). Consequently, the cytoplasmic half of TM6 rotates inward rather than tilting outward. Notably, crystal structures of NAM-bound inactive mGlu1 and mGlu5 7TMs reveal outward-facing W<sup>6.50</sup> conformations similar to inactive CaSR<sup>27,28</sup>. Furthermore, in mGlu2-G<sub>i</sub>, W<sup>6.50</sup> points inward in the G<sub>i</sub>-coupling protomer (companion manuscript). Thus, family C GPCRs utilize a distinct mechanism to couple to G proteins compared to most family A GPCRs, characterized by W<sup>6.50</sup> toggle switch moving inward upon activation.

## Conclusion

Our cryo-EM structures of CaSR in distinct states reveal that receptor activation engenders intrinsic 7TM asymmetry in the homodimer that favors one protomer for G protein-coupling. 7TM PAM binding stabilizes this asymmetry whereas NAM binding locks the 7TMs in a symmetric configuration (Extended Data Fig. 10). Furthermore, comparison between inactive and active CaSR structures reveals that the TM6 toggle switch, conserved across a large number of GPCRs, moves in a different direction upon activation compared to many family A GPCRs. Moreover, our structures reveal at high resolution how various drug molecules target CaSR at either the 7TM or ECD, illustrating the intricate binding mechanisms of CaSR allosteric modulators and yielding valuable insights for the design of improved therapeutics.

## References

1. Hannan, F. M., Kallay, E., Chang, W., Brandi, M. L. & Thakker, R. V. The calcium-sensing receptor in physiology and in calcitropic and noncalcitropic diseases. *Nat Rev Endocrinol* **15**, 33–51 (2019).
2. Møller, T. C., Moreno-Delgado, D., Pin, J.-P. & Kniazeff, J. Class C G protein-coupled receptors: reviving old couples with new partners. *Biophys Rep* **3**, 57–63 (2017).
3. Conigrave, A. D., Quinn, S. J. & Brown, E. M. l-Amino acid sensing by the extracellular Ca<sup>2+</sup>-sensing receptor. *PNAS* **97**, 4814–4819 (2000).
4. Riccardi, D. & Martin, D. The Role of the Calcium-Sensing Receptor in the Pathophysiology of Secondary Hyperparathyroidism. *NDT Plus* **1**, i7–i11 (2008).
5. Nemeth, E. F., Van Wagenen, B. C. & Balandrin, M. F. Discovery and Development of Calcimimetic and Calcilytic Compounds. in *Progress in Medicinal Chemistry* vol. 57 1–86 (Elsevier, 2018).
6. Geng, Y. *et al.* Structural mechanism of ligand activation in human calcium-sensing receptor. *eLife* **5**, e13662 (2016).
7. Zhang, C. *et al.* Structural basis for regulation of human calcium-sensing receptor by magnesium ions and an unexpected tryptophan derivative co-agonist. *Sci Adv* **2**, (2016).
8. Koehl, A. *et al.* Structural Insights into Metabotropic Glutamate Receptor Activation. *Nature* **566**, 79–84 (2019).
9. Fantini, J. & Barrantes, F. J. How cholesterol interacts with membrane proteins: an exploration of cholesterol-binding sites including CRAC, CARC, and tilted domains. *Front. Physiol.* **4**, (2013).
10. Isberg, V. *et al.* Generic GPCR Residue Numbers - Aligning Topology Maps Minding The Gaps. *Trends Pharmacol Sci* **36**, 22–31 (2015).
11. Kifor, O., Diaz, R., Butters, R., Kifor, I. & Brown, E. M. The Calcium-sensing Receptor Is Localized in Caveolin-rich Plasma Membrane Domains of Bovine Parathyroid Cells. *J. Biol. Chem.* **273**, 21708–21713 (1998).
12. Timmers, H. J. L. M., Karperien, M., Hamdy, N. a. T., Boer, H. D. & Hermus, A. R. M. M. Normalization of serum calcium by cinacalcet in a patient with hypercalcaemia due to a de novo inactivating mutation of the calcium-sensing receptor. *Journal of Internal Medicine* **260**, 177–182 (2006).

13. Kunishima, N. *et al.* Structural basis of glutamate recognition by a dimeric metabotropic glutamate receptor. *Nature* **407**, 971–977 (2000).
14. Liu, H. *et al.* Illuminating the allosteric modulation of the calcium-sensing receptor. *PNAS* **117**, 21711–21722 (2020).
15. Bushinsky, D. A. *et al.* One-year safety and efficacy of intravenous etelcalcetide in patients on hemodialysis with secondary hyperparathyroidism. *Nephrology Dialysis Transplantation* **35**, 1769–1778 (2020).
16. Alexander, S. T. *et al.* Critical Cysteine Residues in Both the Calcium-Sensing Receptor and the Allosteric Activator AMG 416 Underlie the Mechanism of Action. *Mol Pharmacol* **88**, 853–865 (2015).
17. Hannan, F. M. *et al.* Identification of 70 calcium-sensing receptor mutations in hyper- and hypo-calcaemic patients: evidence for clustering of extracellular domain mutations at calcium-binding sites. *Hum Mol Genet* **21**, 2768–2778 (2012).
18. Robertson, M. J., van Zundert, G. C. P., Borrelli, K. & Skiniotis, G. GemSpot: A Pipeline for Robust Modeling of Ligands into Cryo-EM Maps. *Structure* **28**, 707-716.e3 (2020).
19. Leach, K. *et al.* Towards a structural understanding of allosteric drugs at the human calcium-sensing receptor. *Cell Res* **26**, 574–592 (2016).
20. Hlavackova, V. *et al.* Evidence for a single heptahelical domain being turned on upon activation of a dimeric GPCR. *The EMBO Journal* **24**, 499–509 (2005).
21. Jacobsen, S. E., Gether, U. & Bräuner-Osborne, H. Investigating the molecular mechanism of positive and negative allosteric modulators in the calcium-sensing receptor dimer. *Scientific Reports* **7**, 46355 (2017).
22. Huang, S. *et al.* Interdomain movements in metabotropic glutamate receptor activation. *Proceedings of the National Academy of Sciences* **108**, 15480–15485 (2011).
23. Ray, K., Fan, G.-F., Goldsmith, P. K. & Spiegel, A. M. The Carboxyl Terminus of the Human Calcium Receptor REQUIREMENTS FOR CELL-SURFACE EXPRESSION AND SIGNAL TRANSDUCTION. *J. Biol. Chem.* **272**, 31355–31361 (1997).
24. Hu, J. *et al.* A Region in the Seven-transmembrane Domain of the Human Ca<sup>2+</sup> Receptor Critical for Response to Ca<sup>2+</sup>. *J. Biol. Chem.* **280**, 5113–5120 (2005).
25. Shiohara, M. *et al.* A novel gain-of-function mutation (F821L) in the transmembrane domain of calcium-sensing receptor is a cause of severe sporadic hypoparathyroidism. *Eur J Pediatr* **163**, 94–98 (2004).

- 1 26. Kobilka, B. K. G protein coupled receptor structure and activation. *Biochimica et Biophysica Acta (BBA) -*  
2 *Biomembranes* **1768**, 794–807 (2007).
- 3 27. Wu, H. *et al.* Structure of a Class C GPCR Metabotropic Glutamate Receptor 1 Bound to an Allosteric  
4 Modulator. *Science* **344**, 58–64 (2014).
- 5 28. Doré, A. S. *et al.* Structure of class C GPCR metabotropic glutamate receptor 5 transmembrane domain. *Nature*  
6 **511**, 557–562 (2014).

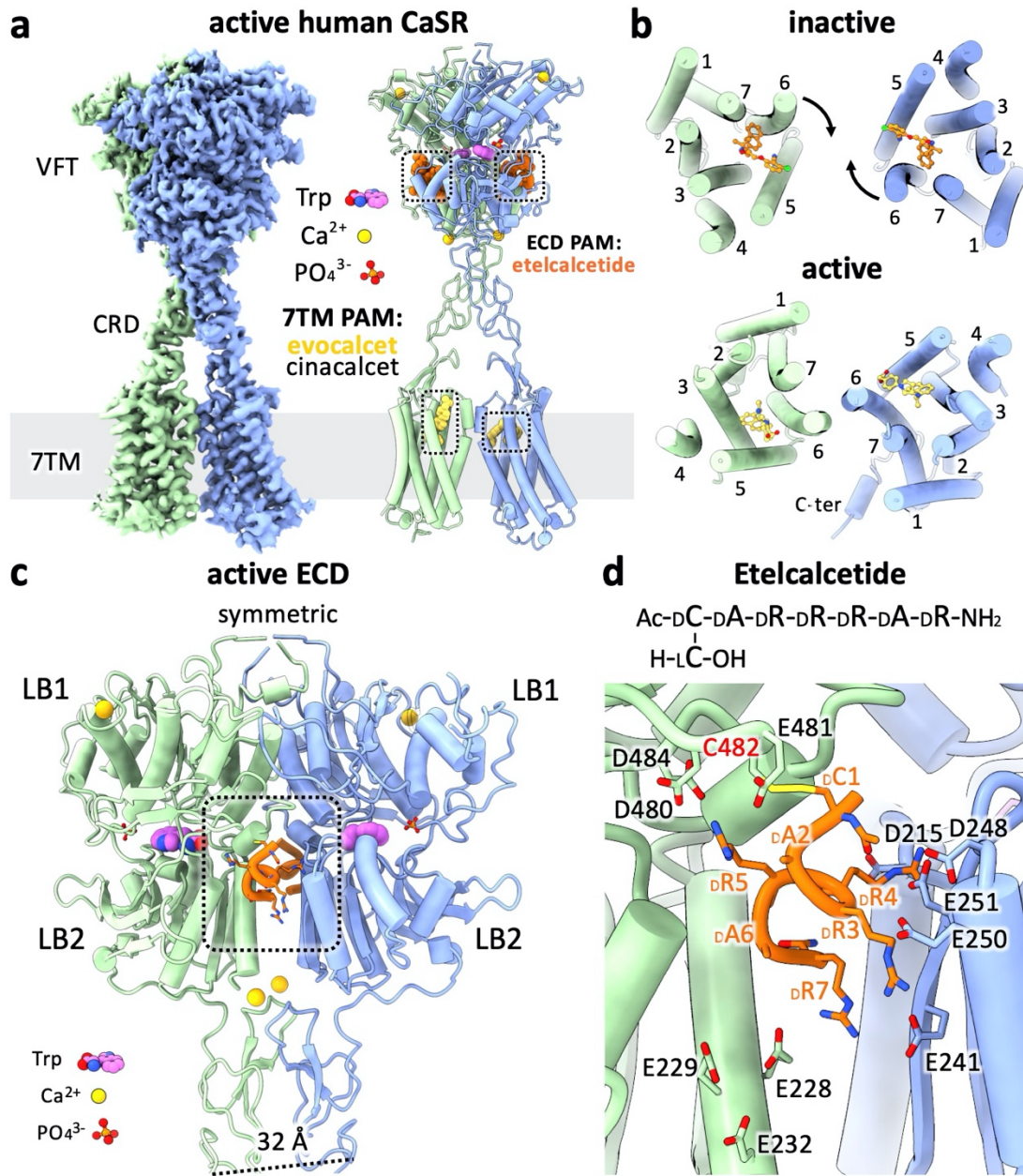
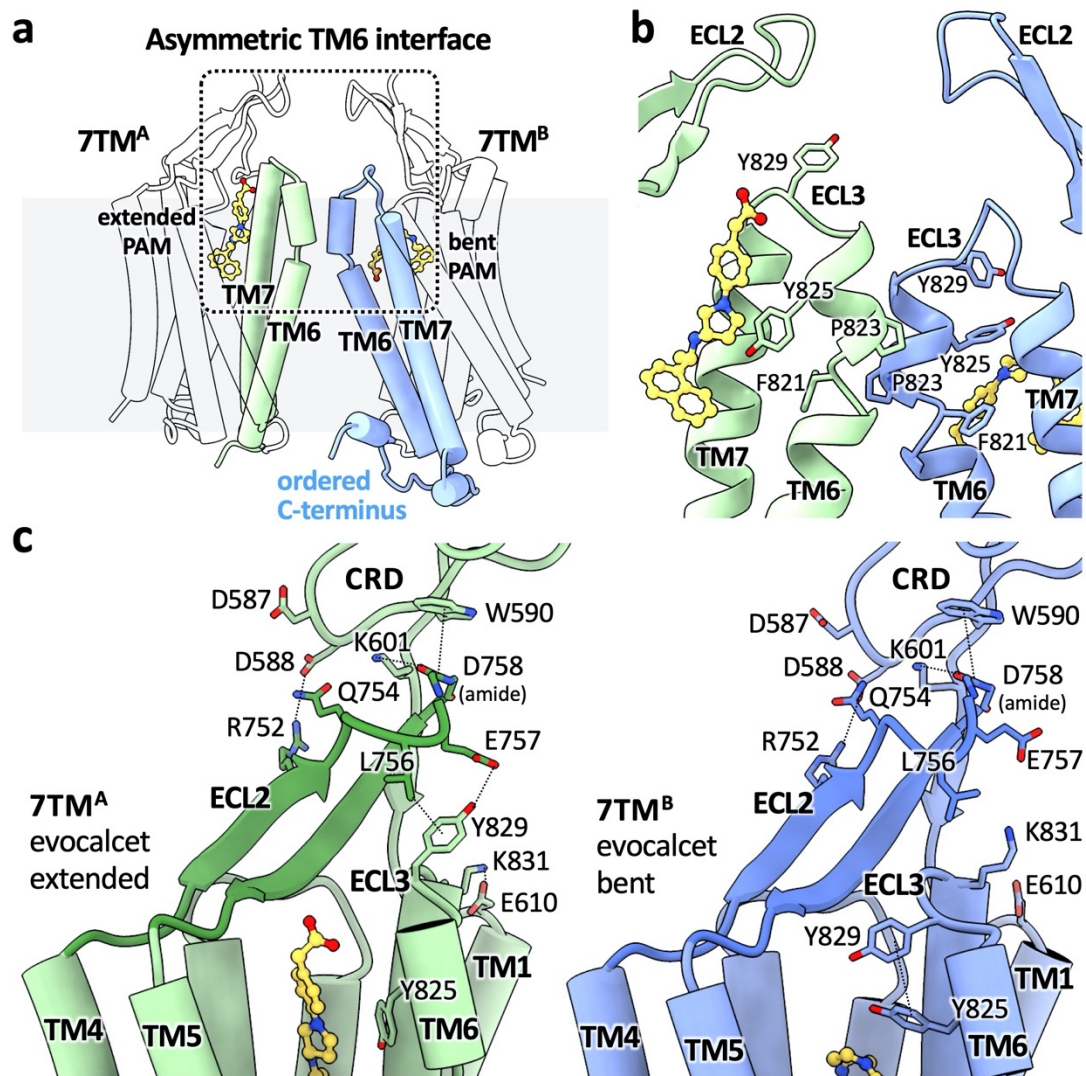
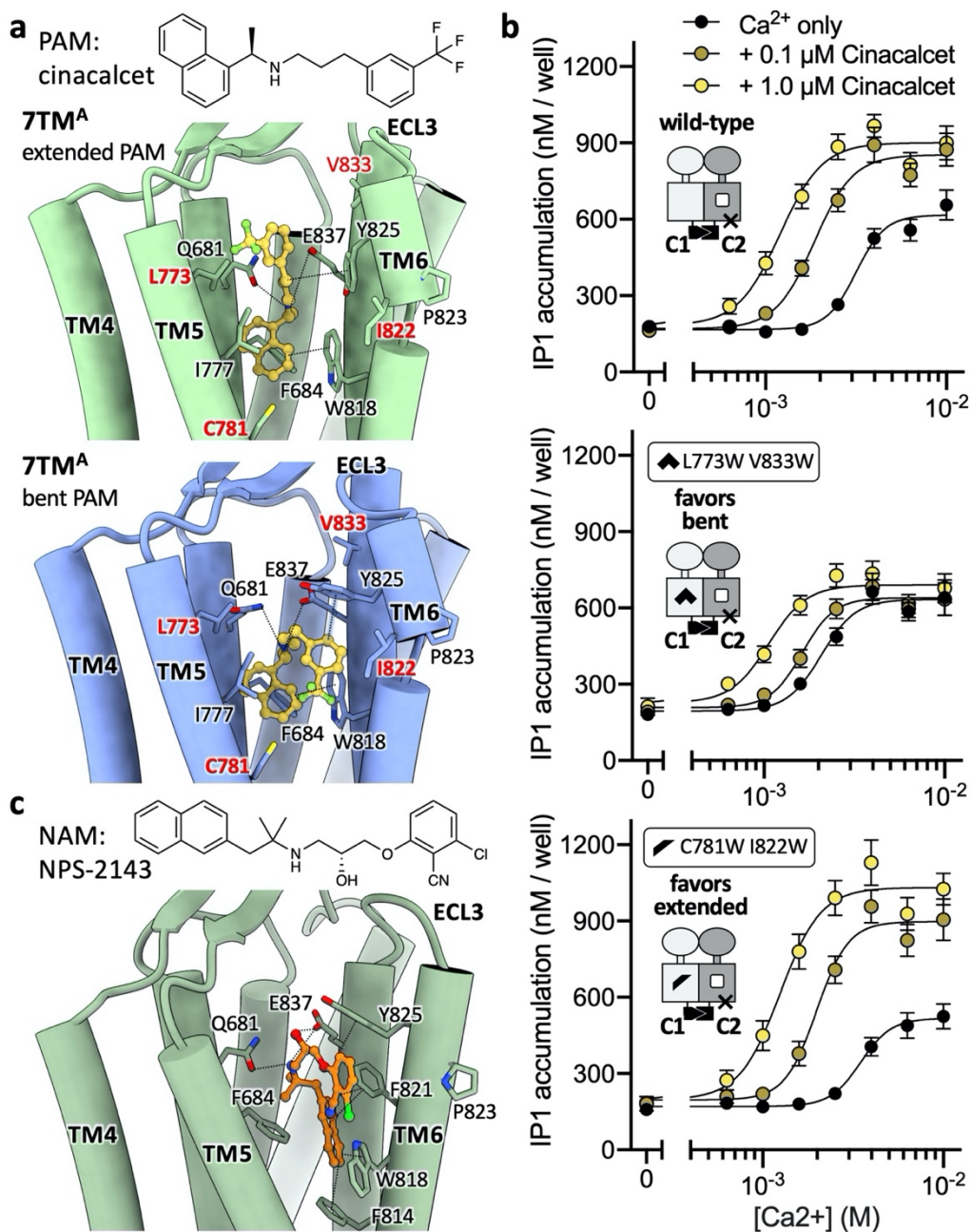


**Figure 1. Structural rearrangements of human CaSR upon activation.** **a**, Cryo-EM map and model of active-state CaSR complexed with evocalcet and etelcalcetide. The PAM cinacalcet binds similarly as evocalcet (Extended Data Figs. 3,6c-d). **b**, Comparison of overall arrangements of 7TM dimer in inactive and active states. **c**, Active-state CaSR ECD complexed with the ECD PAM etelcalcetide (dashed square). **d**, Interactions between etelcalcetide and active-state VFTs.



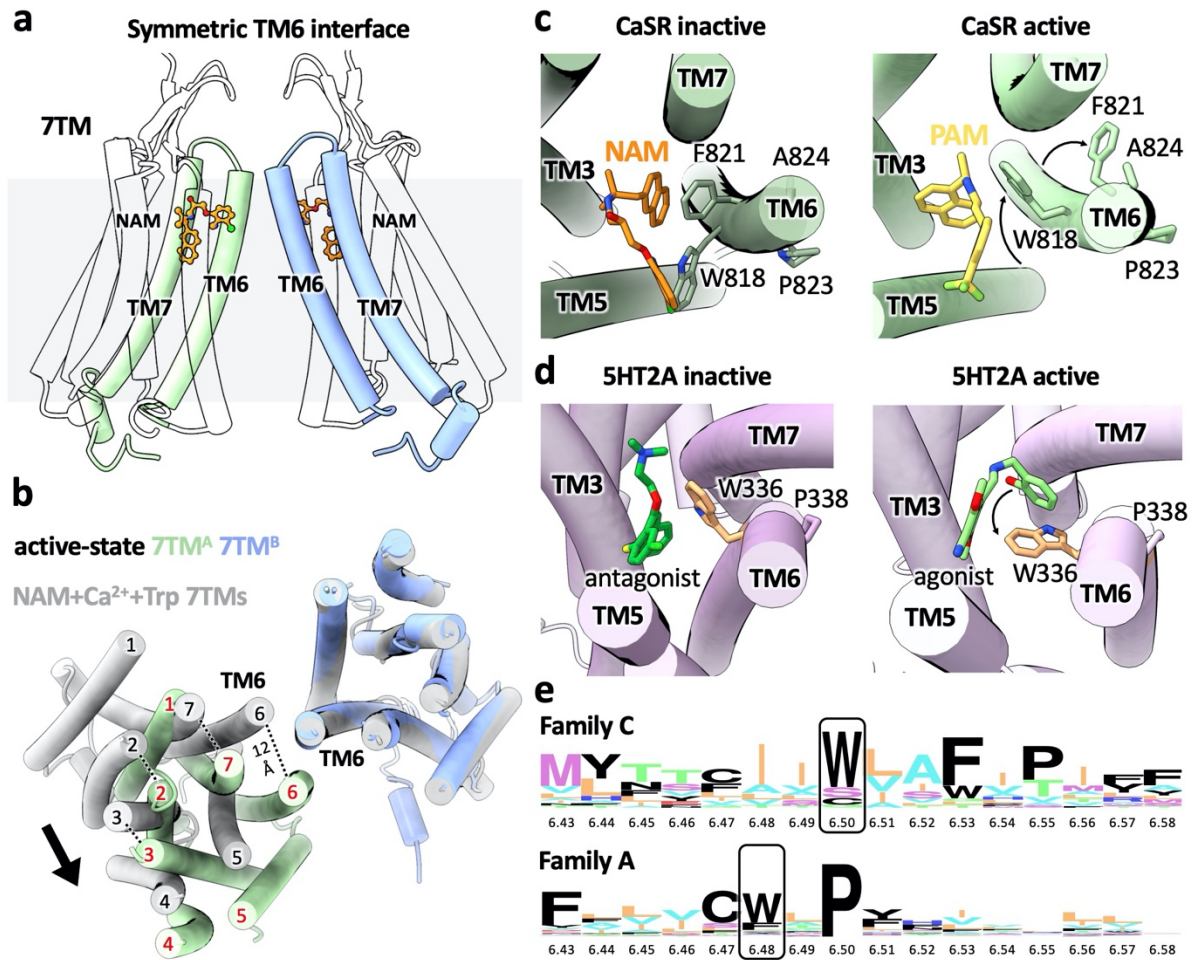
1 **Figure 2. Asymmetric configuration of active-state CaSR 7TMs and interactions between**  
 2 **CRD and 7TM. a, Overall conformation of the asymmetric 7TMs. b, Asymmetric TM6-TM6**  
 3 **interface. c, Interaction network in the CRD-ECL2-ECL3 region of active-state CaSR.**





1 **Figure 3. Structural basis of CaSR-targeting by allosteric calcimimetic (PAM) and calcilytic**  
2 **(NAM) drug molecules. a**, Structure of active-state CaSR 7TMs complexed with cinacalcet. **b**,  
3 IP<sub>1</sub> accumulation assays monitoring Ca<sup>2+</sup> responses for wild-type or PAM-conformer-occlusion  
4 mutants of the CaSR heterodimer with GABA<sub>B</sub> receptor C-terminal tails, in the absence or  
5 presence of the PAM cinacalcet. Data represent mean ± s.e.m. from five independent experiments  
6 each performed in duplicate. **c**, Binding mode of NPS-2143 in the CaSR-NAM-Ca<sup>2+</sup>-Trp 7TM.





1 **Figure 4. Symmetric configuration of CaSR-NAM-Ca<sup>2+</sup>-Trp 7TMs and the TM6 toggle**  
2 **switch.** **a**, Overall structure of symmetric CaSR-NAM-Ca<sup>2+</sup>-Trp 7TMs. **b**, Comparison between  
3 the symmetric CaSR-NAM-Ca<sup>2+</sup>-Trp 7TMs (grey) and the asymmetric PAM-bound 7TMs (7TM<sup>A</sup>  
4 green, 7TM<sup>B</sup> blue) based on 7TM<sup>B</sup> alignment. **c**, Conformational changes in CaSR TM6. **d**,  
5 Conformational changes in serotonin 5HT2A receptor (PDB: 6A94 and 6WHA), a family A GPCR  
6 that couples to G<sub>q</sub>, similarly to CaSR. **e**, Sequence logo of family C and family A TM6 regions  
7 highlighting the conservation of toggle switch motif residues.

## 1    **Methods**

### 2    **Expression and purification of CaSR**

3    Human CaSR (Uniprot: P41180, residues 20-894) with N-terminal influenza haemagglutinin  
4    signal sequence (MKTIIALSYIFCLVFA) followed by FLAG tag (DYKDDDDK) and three Ala  
5    linker (replacing the native signal sequence, residues 1-19) was cloned into either the BamH1 site  
6    of a pFastBac1 vector (Invitrogen) (for insect cell expression) or the BamH1 site of a pcDNA3.1(+)  
7    vector (Thermo Fisher) (for transient transfection of HEK293 cells in cell signaling assays  
8    described in subsequent sections) with InFusion cloning (Takara Bio). CaSR has a large extended  
9    C-terminal domain (residues 864-1078) that is predicted to be unstructured. Most of the flexible  
10    CaSR C-terminus (residues 895-1078) was removed in our construct. Previous studies have shown  
11    that truncation at a position (888) that is N-terminal to our truncation site (894) has no effect on  
12    CaSR signaling<sup>23</sup> and cell-signaling assay results monitoring either direct G protein-coupling or  
13    downstream signaling (IP<sub>1</sub> accumulation) show that our CaSR expression construct is fully  
14    functional (Extended Data Fig. 1b-f).

15    CaSR was expressed in *Spodoptera frugiperda* Sf9 insect cells using the Bac-to-Bac system  
16    (Invitrogen). Sf9 cells cultured in ESF921 medium to a density of  $3.0 \times 10^6$  cells·ml<sup>-1</sup> were infected  
17    with 1% culture volume of P2 baculovirus. Cells were harvested after 48-60h post infection and  
18    washed once with HBS (20 mM HEPES 7.5, 150 mM NaCl). The pellets were snap-frozen in  
19    liquid nitrogen and stored at -80°C.

20    For the purification of inactive-state CaSR, cell pellets were thawed in HBS with 0.5 mM CaCl<sub>2</sub>,  
21    1 mM sodium phosphate (pH 7.5), protease inhibitors, benzonase and 20 μM NPS-2143 (CAS  
22    Number 324523-20-8, Cayman Chemical 17903, prepared as a 20 mM DMSO stock), and lysed  
23    by nitrogen cavitation at 600 psi. The lysate was centrifuged at 1000 x g for 10 min to remove

1 unbroken cells and nuclei, and the membrane fraction was harvested by centrifugation at 100,000  
2 x g for 30 min and solubilized in the same buffer with the addition of 1% DDM and 0.2%  
3 cholesterol hemisuccinate (CHS) for 2 hrs, followed by centrifugation at 100,000 x g for 30 min.  
4 The resulting supernatant was collected and incubated with Anti-DYKDDDDK G1 affinity resin  
5 (GenScript) for 2 hrs or overnight using a batch process. The resin was washed in the same buffer  
6 with 0.1% DDM 0.02% CHS three times and transferred onto a gravity flow column. The column  
7 was washed with 10 column volumes of the same buffer and then the detergent was gradually  
8 exchanged to 0.1% GDN 0.01% CHS. The detergent concentration was then lowered to 0.005%  
9 GDN, 0.0005% CHS and FLAG-tagged CaSR was eluted from the column with the same buffer  
10 containing 0.2 mg/mL FLAG peptide (GenScript). The eluate was concentrated to 500  $\mu$ L with a  
11 100 kDa MWCO Amicon concentrator (Millipore Sigma) and injected onto a Superose6 column  
12 preequilibrated with buffer containing 20 mM HEPES 7.5, 150 mM NaCl, 0.5 mM CaCl<sub>2</sub>, 1 mM  
13 sodium phosphate (pH 7.5), 20  $\mu$ M NPS-2143 and 0.005% GDN, 0.0005% CHS. Peak fractions  
14 were pooled and concentrated to about 7 mg/mL with a 100 kDa MWCO concentrator.  
15 The CaSR-NAM-Ca<sup>2+</sup>-Trp complex was purified in a similar procedure as for the inactive state  
16 with the only difference being that 10 mM CaCl<sub>2</sub>, 10 mM L-Trp, instead of 0.5 mM CaCl<sub>2</sub>, 1 mM  
17 sodium phosphate (pH 7.5), was used throughout the lysis, solubilization and purification.  
18 The active-state CaSR was purified in a similar procedure as for the inactive state. The only  
19 difference is that 10 mM CaCl<sub>2</sub>, 10 mM L-Trp and 20  $\mu$ M of cinacalcet (CAS Number 364782-  
20 34-3, Sigma-Aldrich SML2012, prepared as a 20 mM DMSO stock) or a combination of 20  $\mu$ M  
21 of evocalcet (CAS Number 870964-67-3, MedChem Express HY-17613, prepared as a 20 mM  
22 DMSO stock) and 50  $\mu$ M etelcalcetide (CAS Number 1334237-71-6, Cayman Chemical 26901,

prepared as a 0.1 mg/ml stock in HBS), instead of 0.5 mM CaCl<sub>2</sub>, 1 mM sodium phosphate (pH 7.5) and 20 μM NPS-2143, were used throughout the lysis, solubilization and purification.

### **Cryo-EM data collection and processing**

3 μL inactive- or active-state CaSR or CaSR-NAM-Ca<sup>2+</sup>-Trp at 7 mg/mL was applied to freshly glow-discharged 300-mesh R1.2/R1.3 UltrAuFoil holey gold grids (Quantifoil) under 100% humidity at 4°C. Excess sample was blotted away for 3 seconds, and the grids were subsequently plunged-frozen into liquid ethane using a Vitrobot Mark IV (Thermo Fisher Scientific) and then stored in liquid nitrogen. For the inactive- or active-state CaSR grids, cryo-EM data was collected on a Titan Krios electron microscope (Thermo Fisher Scientific - FEI) operating at 300 kV with a calibrated magnification of x81,000, corresponding to a pixel size of 1.11 Å. Micrographs were recorded using a K3 direct electron camera (Gatan) with a dose rate of 16.23 electrons·Å<sup>-2</sup>·sec<sup>-1</sup> and defocus values ranging from -0.7 μm to -1.5 μm. The total exposure time was 4 sec and intermediate frames were recorded in 0.05 sec intervals, resulting in an accumulated dose of 64.9 electrons·Å<sup>-2</sup> and a total of 80 frames per micrograph. For the CaSR-NAM-Ca<sup>2+</sup>-Trp grid, cryo-EM data was collected on a Titan Krios electron microscope (Thermo Fisher Scientific - FEI) operating at 300 kV with a calibrated magnification of x105,000, corresponding to a pixel size of 0.8677 Å. Micrographs were recorded using a K3 direct electron camera (Gatan) with a dose rate of 24.36 electrons·Å<sup>-2</sup>·sec<sup>-1</sup> and defocus values ranging from -0.8 μm to -1.8 μm. The total exposure time was 2.5 sec and intermediate frames were recorded in 0.05 sec intervals, resulting in an accumulated dose of 60.9 electrons·Å<sup>-2</sup> and a total of 50 frames per micrograph. Cryo-EM data processing was done in cryoSPARC v3.0 (inactive- or active-state CaSR) or v3.1 (CaSR-NAM-Ca<sup>2+</sup>-Trp )<sup>29</sup> (Extended Data Fig. 2). Dose fractionated image stacks were subjected to beam-induced motion correction and filtering with patch motion correction and CTF parameters

1 were refined with patch CTF refinement. Auto-picked particle projections were extracted and  
2 subjected to several rounds of reference-free 2D classification. Five initial models were generated  
3 for each dataset with 3D *ab initio* reconstruction and the particles were subjected to several rounds  
4 of 3D heterogeneous refinement to remove particles populating poorly defined classes. Particles  
5 from conformationally homogeneous groups were then subjected to local motion correction,  
6 followed by local and global CTF refinement. Subsequently, the particles were subjected to several  
7 rounds of further 2D classification and 3D heterogeneous refinement. The resulting particles were  
8 refined with nonuniform refinement<sup>30</sup> followed by local nonuniform refinement with a soft mask  
9 around either the ECD or 7TM regions (Extended Data Figs. 3-4). For the CaSR-NAM-Ca<sup>2+</sup>-Trp,  
10 local refinement without symmetry at the 7TMs yielded a fully symmetric map at 3.4 Å, and C2  
11 symmetry was then applied to subsequent refinement of this region improving the resolution to 3.3  
12 Å (Extended Data Fig. 4).

13 We carried out 3D variability analysis<sup>31</sup> in cryoSPARC v3.0 with particles after local motion  
14 correction (inactive-state CaSR dataset) or after local and global CTF refinement (dataset of active-  
15 state CaSR with evocalcet and etelcalcetide). The particles were subjected to one round of 2D  
16 classification and then subjected to nonuniform refinement to generate the 3D reference and mask  
17 for the 3D variability analysis with three principal components. The series of frames from motions  
18 corresponding to each principal component were visualized as movies in UCSF Chimera<sup>32</sup>  
19 (Supplementary Videos 1-3 for inactive CaSR and Supplementary Videos 4-6 for active CaSR).  
20 In the inactive state, CaSR is relatively flexible, and our structure reveals an asymmetric open-  
21 closed conformation of the ECD stabilized by what appears to be an aromatic amino acid or its  
22 derivatives. Given that a previous crystal structure of the inactive CaSR ECD depicts a symmetric  
23 open-open conformation, it is possible that the receptor exists in an equilibrium of these two

conformations under low calcium conditions (Extended Data Fig. 10). Indeed, our 3D variability analysis of inactive-state CaSR reveals significant breathing of the VFTs accompanied by back-and-forth flexing relative to the 7TMs (Supplementary Videos 1-3). The same analysis for the active state shows that the VFTs adopt a rigid closed-closed conformation and flex around the CRDs (Supplementary Videos 4-6). Interestingly, the first principal component of the movements in the active state (Supplementary Video 4) reveals a tug-of-war like motion of the 7TMs alternatively pushing each other to adopt a tilted conformation, reminiscent to the bent PAM protomer in our structures that disfavors G protein-coupling. This motion suggests that 7TMs may stochastically alternate to activate one G protein at a time, a mechanism previously proposed for various family C GPCRs based on cell signaling studies<sup>20,21,33</sup>.

## **Model building and refinement**

The crystal structures of active and inactive CaSR ECD<sup>6</sup> (PDB: 5K5S and 5K5T) together with homology models of CaSR 7TM based on the active and inactive mGlu5 cryo-EM structures<sup>8</sup> (PDB: 6N51 and 6N52) calculated with SWISS-MODEL<sup>34</sup> were used as initial models and manually docked into cryo-EM densities with Chimera<sup>32</sup>. The models were then subjected to iterative rounds of automated refinement using Phenix real space refine<sup>35</sup>, and manual building in Coot<sup>36</sup>. Poses of small molecule PAMs and NAM were generated with GemSpot<sup>18</sup> and the model of the poly-D peptide etelcalcetide was manually built in Coot. The final models were subjected to global refinement and minimization in real space in Phenix. Validation was performed in MolProbity<sup>37</sup> and EMRinger<sup>38</sup>. The refinement statistics are provided in Supplementary Table S1.

## **BRET2 assays for CaSR-G<sub>q</sub> signaling**

BRET2 assays were performed using TRUPATH reagents as previously described<sup>39</sup> with some modifications. HEK-293S cells in FreeStyle suspension media (Thermo Fisher) were transiently

transfected at a density of 1 million cells·mL<sup>-1</sup> with a 1:1:1:1 ratio of CaSR (pcDNA 3.1 (+) construct described in the first method section) : Gα-RLuc8 : Gβ : Gγ-GFP, using polyethyleneimine. Cells were harvested by centrifugation 48 hours later and resuspended in assay buffer (HBSS + 20 mM HEPES pH 7.5) at a density of 1.25 million cells·mL<sup>-1</sup>, which was then plated in white 96-well assay plates (Corning) at 40 µl per well. After the addition of 20 ul of freshly prepared 30 µM coelenterazine 400a (GoldBio, St Louis, MO), plates were incubated for five minutes, treated with 30 µl of ligand for an additional five minutes, and read in a SpectraMax iD5 plate reader (Molecular Devices, San Jose, CA) with 410 nm and 515 nm emission filters with a 1 sec per well integration time. BRET2 ratios (Net BRET) were calculated as the ratio of GFP2 emission (515 nm) to RLuc8 emission (410 nm) and analyzed in GraphPad Prism version 9.0.0 for Mac (GraphPad Software, San Diego, CA).

#### **IP<sub>1</sub> assay for profiling of allosteric modulators**

Human embryonic kidney (HEK) cells were cultured in DMEM (Gibco, Thermo Fisher Scientific) supplemented with 10% v/v dFBS and 1% v/v at 37°C, and 5% CO<sub>2</sub>. The cells were transiently transfected with the pcDNA 3.1 (+) construct encoding human CaSR (20-894 with N-terminal HA signal sequence, FLAG-tag and a three Ala linker) using linear PEI as transfection reagent (250 ng vector DNA/million cells; 1:4 ratio with PEI). 24 hours post transfection, cells (40,000 cells/well) were seeded in poly-D-lysine treated 96-well tissue culture plates (Corning) and incubated overnight at 37°C and 5% CO<sub>2</sub>. The IP<sub>1</sub> experiments were performed using the IP-One assay (Cisbio) as previously described<sup>21</sup>. In brief, cells were washed once with HBSS (no Ca, Mg, Gibco 14175) supplemented with 20 mM HEPES pH 7.4 and then incubated with compounds prepared in the same buffer additionally supplemented with 20 mM LiCl for 30 min at 37°C. After incubation, the cells were washed with assay buffer and lysed using IP-One Conjugate & Lysis

1 buffer (Cisbio). Cell lysates (10  $\mu$ l/well) were subsequently transferred to a 384-well Optiplate  
2 (Perkin Elmer), after which (10  $\mu$ l/well) detection solution (lysis buffer, 2.5% v/v anti-IP<sub>1</sub> antibody  
3 cryptate Terbium-conjugate, 2.5% v/v IP<sub>1</sub>-d2 conjugate) was added to the cell lysates. The plate  
4 was incubated for 1 hour at RT (in the dark) and subsequently measured on the Envision plate  
5 reader (Perkin Elmer).

## 6 **Generation of forced CaSR dimer constructs and mutagenesis**

7 The pcDNA 3.1(+) construct encoding human CaSR as described in the first method section was  
8 used as the template for the generation of CaSR constructs with either GABA<sub>B1</sub> or GABA<sub>B2</sub> C-  
9 terminus (C1 or C2). For the CaSR-C1 construct, DNA encoding the sequence of  
10 TGSSTNNNEEEKSRLLLEKENRELEKIIAEKEERVSELRHQLQSRQQL**KKTN** was inserted in  
11 between CaSR residue 894 and the stop codon with restriction-free (rf) cloning<sup>40</sup>. For the CaSR-  
12 C2, a TSTSVTSVNQASTSRLEGLQSENHRLRMKITELDKDL EEV T MQLQDTPE**KKTN**  
13 sequence was inserted in between CaSR residue 894 and the stop codon and the N-terminal FLAG-  
14 tag was replaced with an HA epitope tag (YPYDVPDYA). Point mutations used in this study were  
15 generated with rf cloning<sup>40</sup>.

## 16 **IP<sub>1</sub> assay for expression of forced CaSR dimers**

17 To determine the functional response of specific combinations of CaSR dimer mutants at the cell  
18 surface, HEK293 cells (ATCC® CRL-1573™) were transfected with FLAG-tagged CaSR-C1 and  
19 HA-tagged CaSR-C2 constructs using FuGene6 (Promega E2692) transfection reagent essentially  
20 as described previously<sup>41</sup>. The absolute amounts of DNA used for each FLAG-tagged CaSR-C1  
21 or HA-tagged CaSR-C2 constructs or their combinations were varied to obtain equal expression  
22 levels of the respective CaSR dimer mutants at the cell surface (amounts given in Extended Data  
23 Fig. 8b). For the Q681A mutation experiments, DNA amount used for the FLAG-tagged WT and



Q681A constructs were 0.015 µg. The total amount of DNA was always 1 µg DNA for each 1 mL of transfected cell suspension and was, if needed, supplemented to 1 µg using empty vector DNA. HEK293 cells were detached and resuspended to 0.28 million cells/mL in growth medium (DMEM, Gibco 10566016; supplemented with 10% Fetal Bovine Serum, Gibco 10270106; 1% Sodium Pyruvate, Gibco 11360039; 1% MEM Non-Essential Amino Acids, Gibco 11140068; and 1% Penicillin-Streptomycin Solution, Gibco 15140122). Following dilution of 3 µL FuGene6 into 57 µL OptiMEM (Gibco 51985) for each 1 mL of cell suspension to be transfected, the 60 µL OptiMEM/FuGene6 mixture was added to a total of 1 µg DNA in 25 µL OptiMEM and incubated for 20 min at room temperature. Then, the mixture of FuGene6 and DNA in OptiMEM was added directly to the cell suspension and seeded in poly-D-lysine coated 96-well plates at a density of 28,000 cells/well in 100 µL. The IP<sub>1</sub> assay was performed as described above for PAM and NAM profiling, except that cells were incubated with Ca<sup>2+</sup> in absence or presence of PAM for 45 min at 37°C, and cells were lysed in 40 µL IP-One Conjugate & Lysis buffer (Cisbio).

#### **Cell surface ELISA assay**

Following transfection of the FLAG-tagged CaSR-C1, HA-tagged CaSR-C2 constructs, their combinations, or FLAG-tagged WT or Q681A mutant as described above, cells were seeded in white clear bottom poly-D-lysine coated 96-well plates, and assayed after 48 hrs. The cell surface ELISA assay to quantify the relative surface expression levels of each of the protomers of the forced mutant CaSR dimers was performed as described previously<sup>41</sup> by detecting the relative surface expression levels of FLAG-tagged C1-mutant protomers and/or HA-tagged C2-mutant protomers relative to high-expressing FLAG-CaSR-WT-C1 and HA-CaSR-F801A-C2 forced dimer (Extended Data Fig. 8b). For the FLAG-tagged WT and Q681A mutant surface expression

1 levels were determined relative to the cell surface ELISA signal of an identical transfection of  
2 FLAG-tagged WT (Extended Data Fig. 8a).

### 3 **Data availability**

4 All data generated or analysed during this study are included in the Article and its Supplementary  
5 Information. Cryo-EM maps of active-state CaSR-cinacalcet, active-state CaSR-etelcalcetide-  
6 evocalcet, inactive-state CaSR-NPS2143 and CaSR-NPS2143-Ca<sup>2+</sup>-Trp have been deposited in  
7 the Electron Microscopy Data Bank under accession codes EMD-23653, EMD-23654, EMD-2365  
8 and EMD-23652, respectively. The atomic coordinates of active-state CaSR-cinacalcet, active-  
9 state CaSR-etelcalcetide-evocalcet, inactive-state CaSR-NPS2143 and CaSR-NPS2143-Ca<sup>2+</sup>-Trp  
10 have been deposited in the Protein Data Bank under the accession codes 7M3F, 7M3G, 7M3J and  
11 7M3E, respectively.

### **References**

- 12 29. Punjani, A., Rubinstein, J. L., Fleet, D. J. & Brubaker, M. A. cryoSPARC: algorithms for rapid unsupervised  
13 cryo-EM structure determination. *Nature Methods* **14**, 290–296 (2017).
- 14 30. Punjani, A., Zhang, H. & Fleet, D. J. Non-uniform refinement: adaptive regularization improves single-particle  
15 cryo-EM reconstruction. *Nature Methods* **17**, 1214–1221 (2020).
- 16 31. Punjani, A. & Fleet, D. J. *3D Variability Analysis: Directly resolving continuous flexibility and discrete*  
17 *heterogeneity from single particle cryo-EM images*. <http://biorxiv.org/lookup/doi/10.1101/2020.04.08.032466>  
18 (2020) doi:10.1101/2020.04.08.032466.
- 19 32. Pettersen, E. F. *et al.* UCSF Chimera--a visualization system for exploratory research and analysis. *J Comput*  
20 *Chem* **25**, 1605–1612 (2004).
- 21 33. Goudet, C. *et al.* Asymmetric Functioning of Dimeric Metabotropic Glutamate Receptors Disclosed by Positive  
22 Allosteric Modulators. *J. Biol. Chem.* **280**, 24380–24385 (2005).

34. Waterhouse, A. *et al.* SWISS-MODEL: homology modelling of protein structures and complexes. *Nucleic Acids Res* **46**, W296–W303 (2018).
35. Adams, P. D. *et al.* PHENIX: a comprehensive Python-based system for macromolecular structure solution. *Acta Cryst D, Acta Cryst Sect D, Acta Crystallogr D, Acta Crystallogr Sect D, Acta Crystallogr D Biol Crystallogr, Acta Crystallogr Sect D Biol Crystallogr* **66**, 213–221 (2010).
36. Emsley, P. & Cowtan, K. Coot: model-building tools for molecular graphics. *Acta Crystallogr. D Biol. Crystallogr.* **60**, 2126–2132 (2004).
37. Chen, V. B. *et al.* MolProbity: all-atom structure validation for macromolecular crystallography. *Acta Cryst D* **66**, 12–21 (2010).
38. Barad, B. A. *et al.* EMRinger: side chain-directed model and map validation for 3D cryo-electron microscopy. *Nature Methods* **12**, 943–946 (2015).
39. Olsen, R. H. J. *et al.* TRUPATH, an open-source biosensor platform for interrogating the GPCR transducerome. *Nature Chemical Biology* **16**, 841–849 (2020).
40. Bond, S. R. & Naus, C. C. RF-Cloning.org: an online tool for the design of restriction-free cloning projects. *Nucleic Acids Res* **40**, W209–W213 (2012).
41. Papasergi-Scott, M. M. *et al.* Structures of metabotropic GABA B receptor. *Nature* **584**, 310–314 (2020).
42. Isberg, V. *et al.* GPCRdb: an information system for G protein-coupled receptors. *Nucleic Acids Res* **44**, D356–D364 (2016).
43. Crooks, G. E. WebLogo: A Sequence Logo Generator. *Genome Research* **14**, 1188–1190 (2004).

## Acknowledgements

We thank Elizabeth Montabana at the Stanford-SLAC cryo-EM facility for support with data collection and Brian Kobilka for comments on the manuscript. This work was supported, in part, by R01 NS092695 (G.S. and J.M.M.) and a grant from the Mathers Foundation (G.S.); a Wellcome Trust Investigator Award (grant number 106995/Z/15/Z) (R.V.T); National Institute for Health Research (NIHR) Oxford Biomedical Research Centre Programme (R.V.T.); NIHR Senior

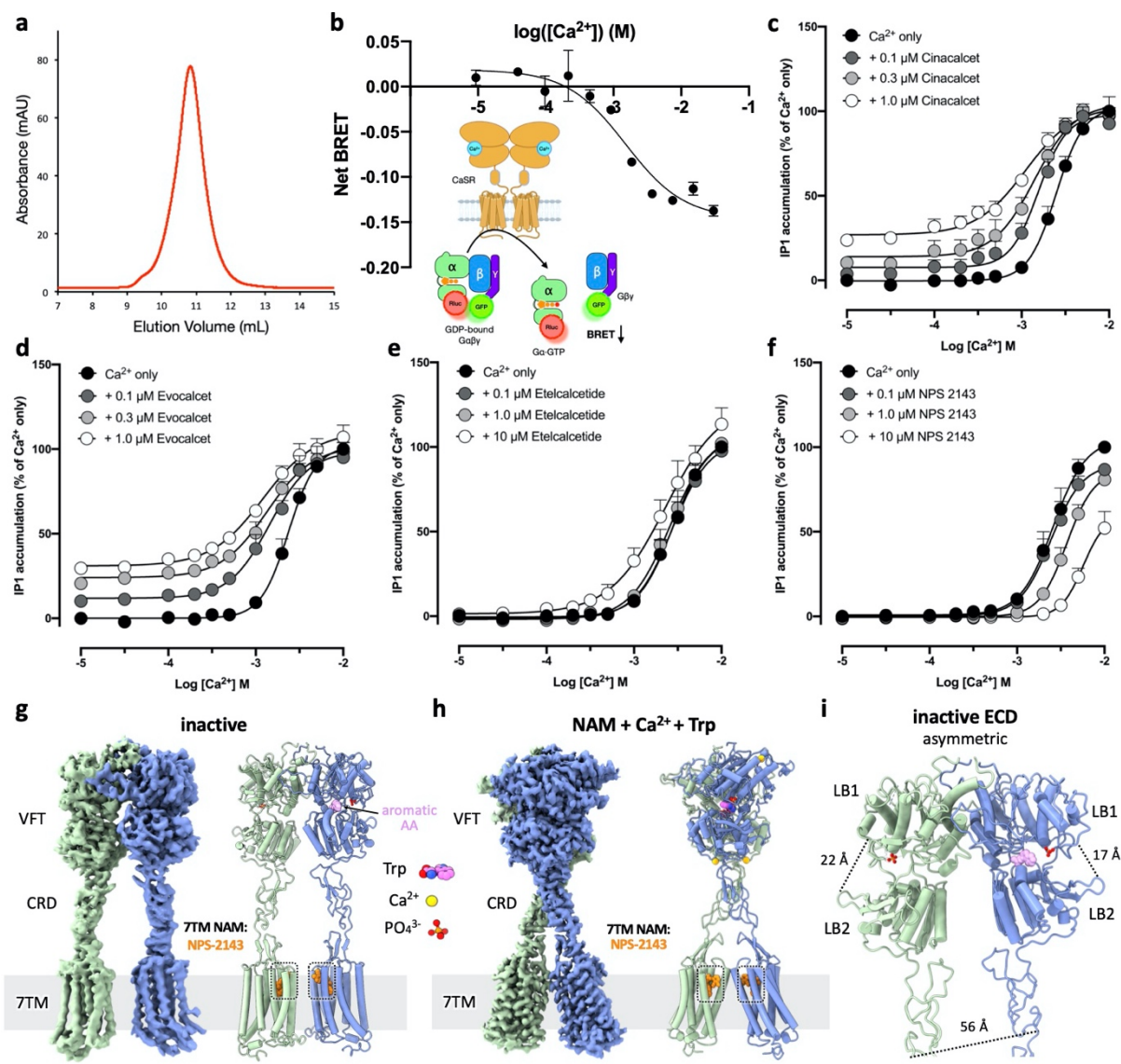
Investigator Award (R.V.T.) (grant number NF-SI-0514–10091); T32-GM089626 (J.G.M.); funding from the Faculty of Health and Medical Sciences (H.B.-O.).

### **Author contributions**

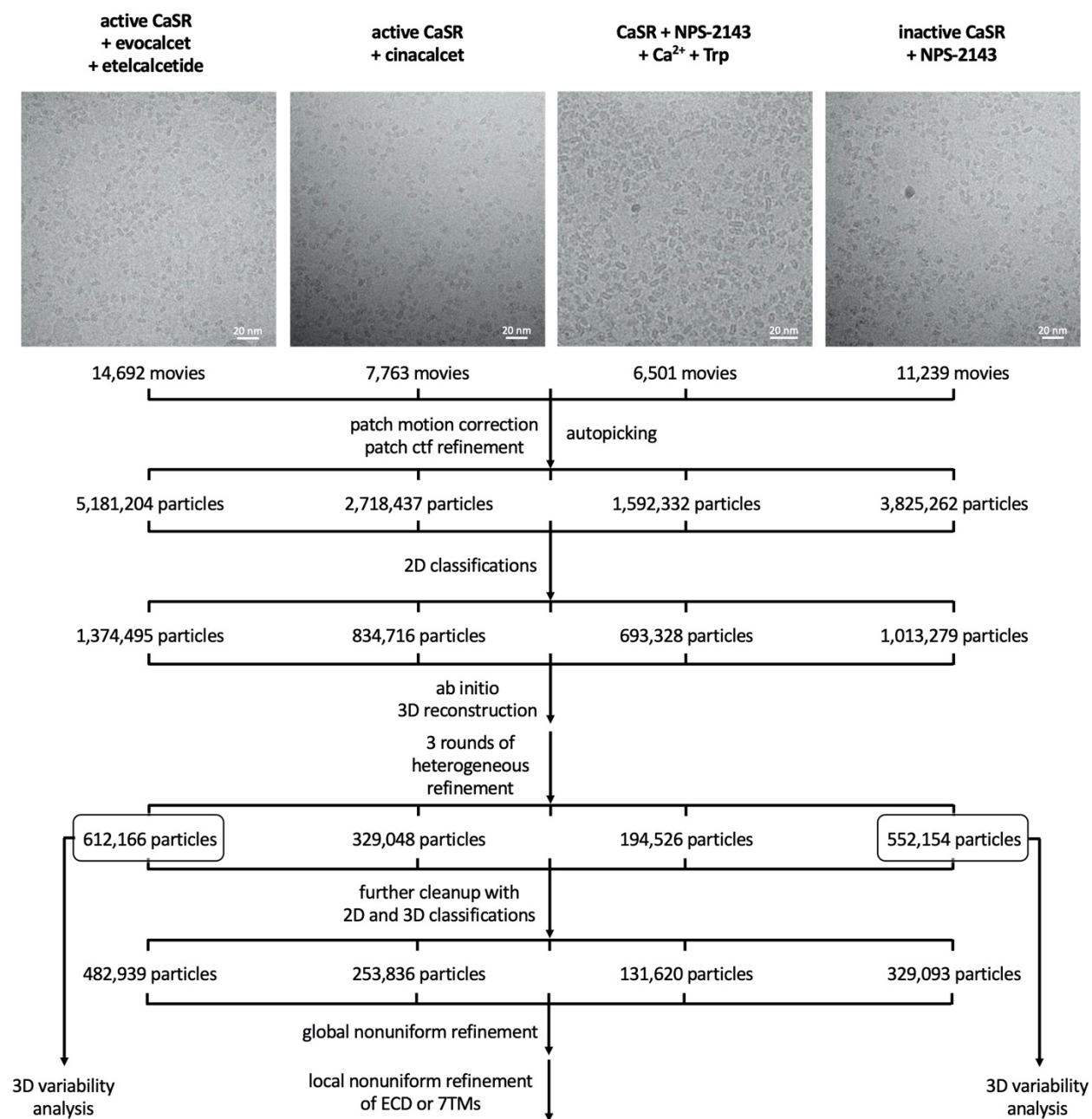
Y.G. expressed and purified the proteins, prepared cryo-EM samples, collected and processed cryo-EM data, built and refined the structural models, designed the mutagenesis studies, generated the expression constructs. M.J.R. performed ligand docking and assisted in model refinement. S.N.R. performed IP<sub>1</sub> assays for profiling of allosteric modulators under the supervision of H.B.O. A.B.S. assisted in data analysis. C.Z. assisted in cryo-EM data collection. J.G.M. performed the BRET assays and assisted in model refinement. O.P. assisted in cryo-EM data collection. F.M.H. and R.V.T. provided information on disease mutations and provided input in manuscript discussions. J.M.M. performed and analyzed cellular signaling experiments. Y.G. and G.S. wrote the manuscript with input from J.G.M, R.V.T., F.M.H., H.B.O, M.J.R., and J.M.M.. G.S. supervised the project.

### **Competing interests**

The authors declare no competing interests.

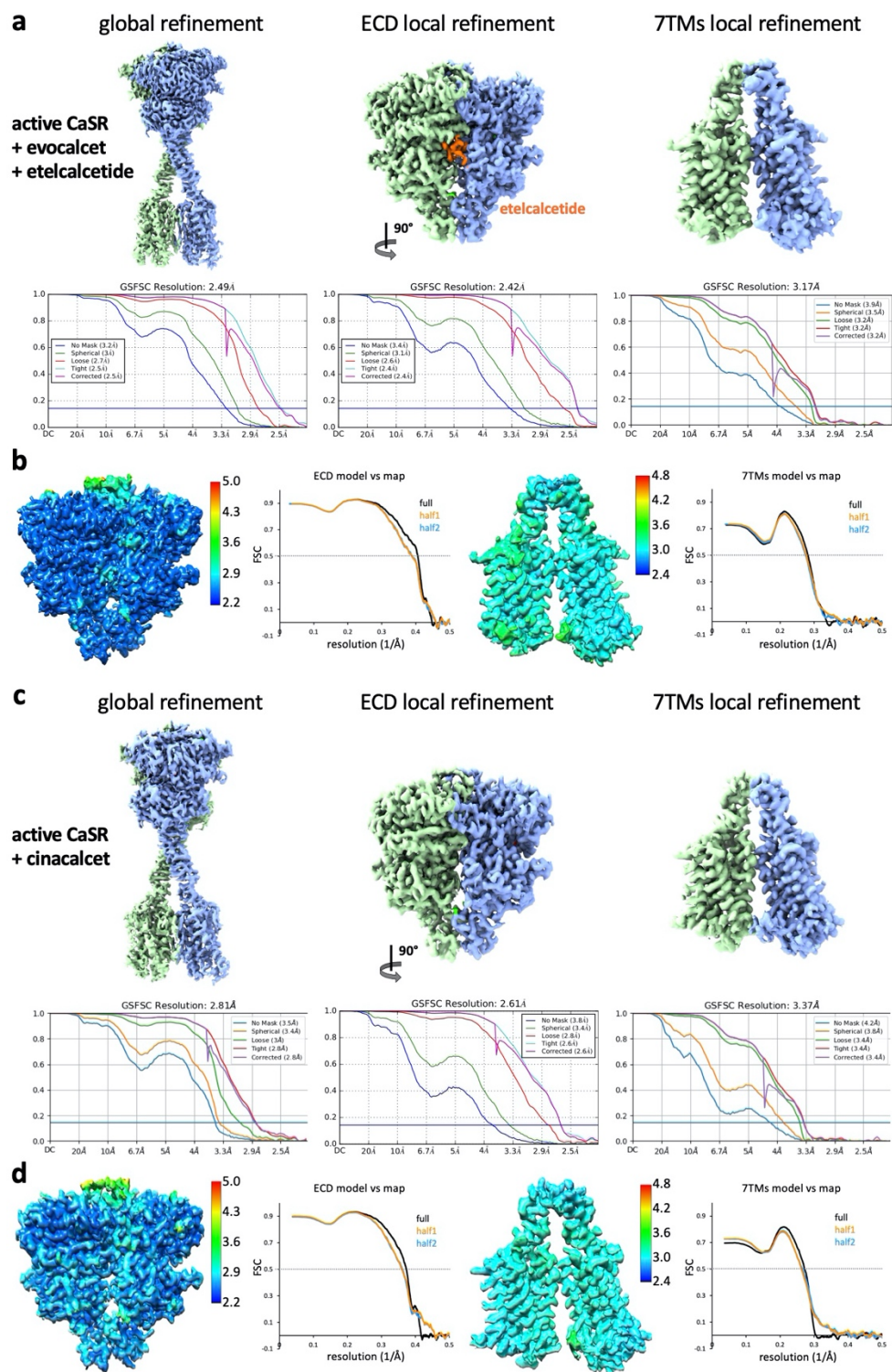


**Extended Data Figure 1. Functional characterizations of human CaSR and Structures of NAM-bound CaSR.** **a**, size-exclusion chromatography profile of purified CaSR. **b**, BRET-based assay<sup>39</sup> monitoring G<sub>q</sub> activation by CaSR upon Ca<sup>2+</sup> addition.  $n=3$  independent experiments, data represent mean  $\pm$  s.e.m. **c-f**, Functional responses of CaSR to Ca<sup>2+</sup> alone or in combination with PAMs or NAM measured by IP<sub>1</sub> accumulation assays.  $n=3$  independent experiments, data represent mean  $\pm$  s.e.m. **g**, Cryo-EM map and model of inactive state CaSR complexed with NAM. **h**, Cryo-EM map and model of the CaSR-NAM-Ca<sup>2+</sup>-Trp complex. **i**, Structure of the inactive-state CaSR ECD region showing an open-closed inactive VFT configuration.

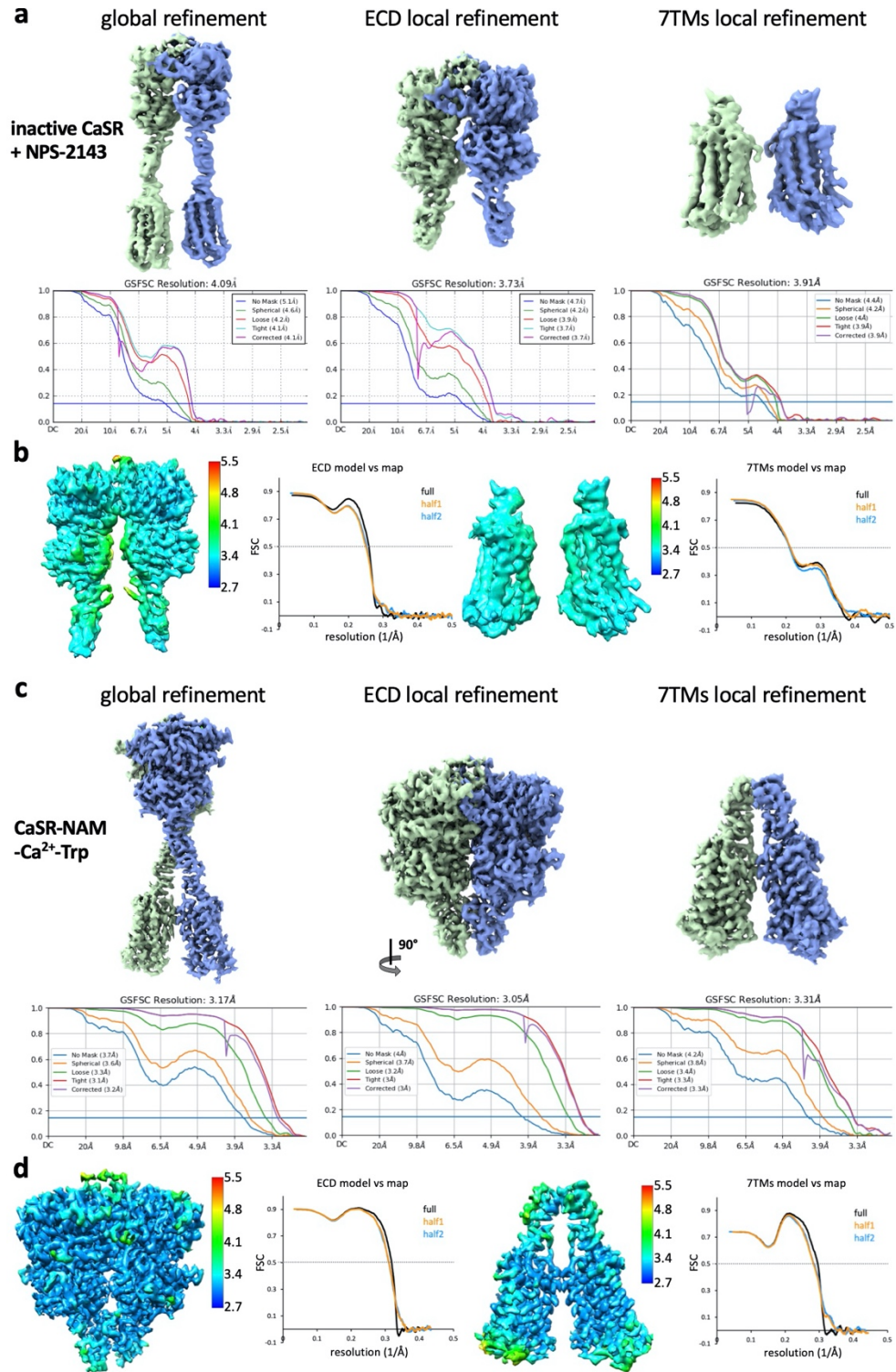


1 Extended Data Figure 2. Cryo-EM data processing workflow.



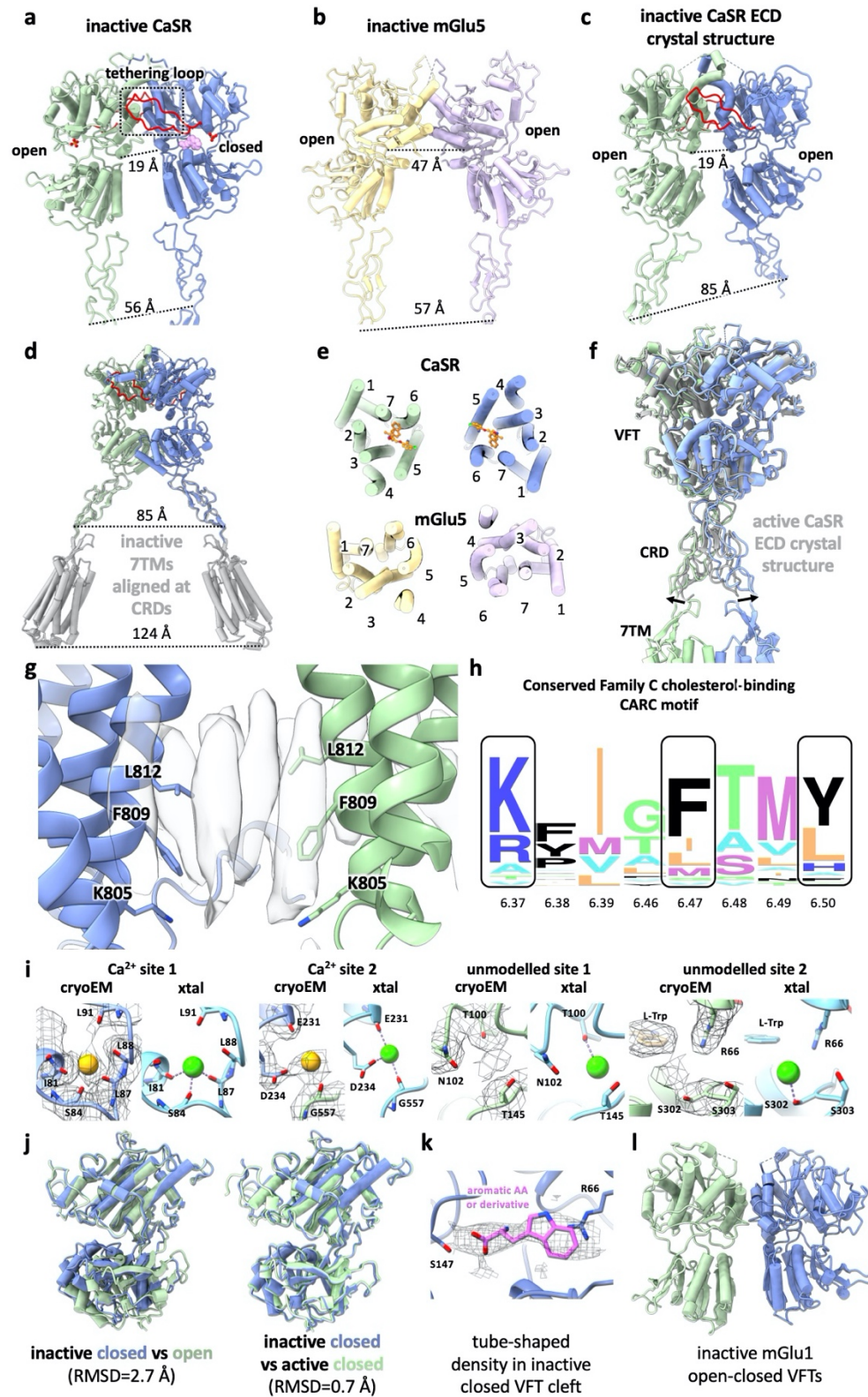


1      Extended Data Figure 3. Global and local refinement maps with corresponding FSC curves  
2      indicating nominal resolutions using the FSC = 0.143 criterion, model-vs-map FSC curves  
3      and local resolution maps of CaSR-etelcalcetide-evocalcet (a-b) and CaSR-cinacalcet (c-d).



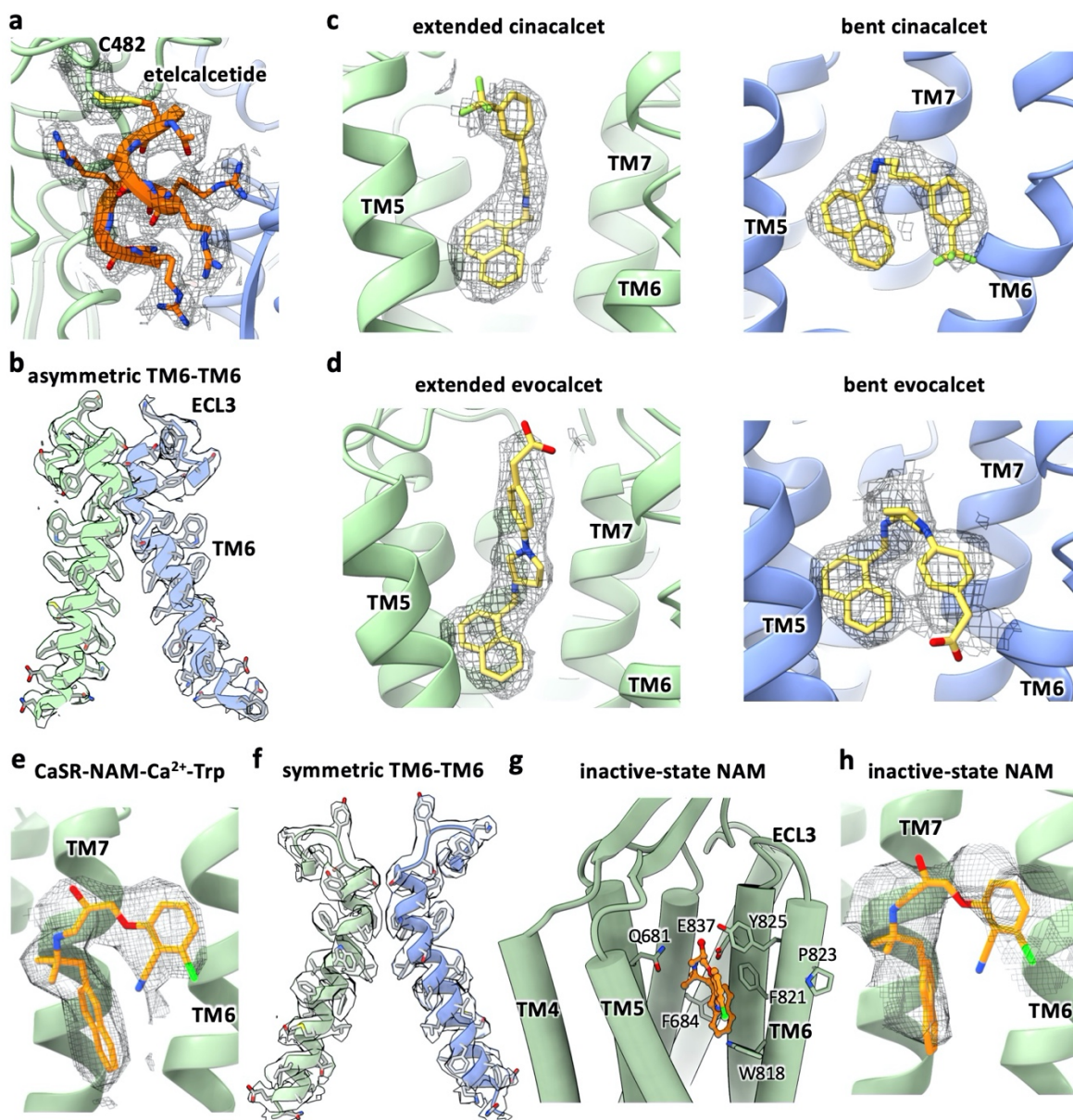
1 Extended Data Figure 4. Global and local refinement maps with corresponding FSC curves  
 2 indicating nominal resolutions using the FSC = 0.143 criterion, model-vs-map FSC curves  
 3 and local resolution maps of inactive-state CaSR (a-b) and CaSR-NAM-Ca<sup>2+</sup>-Trp (c-d).





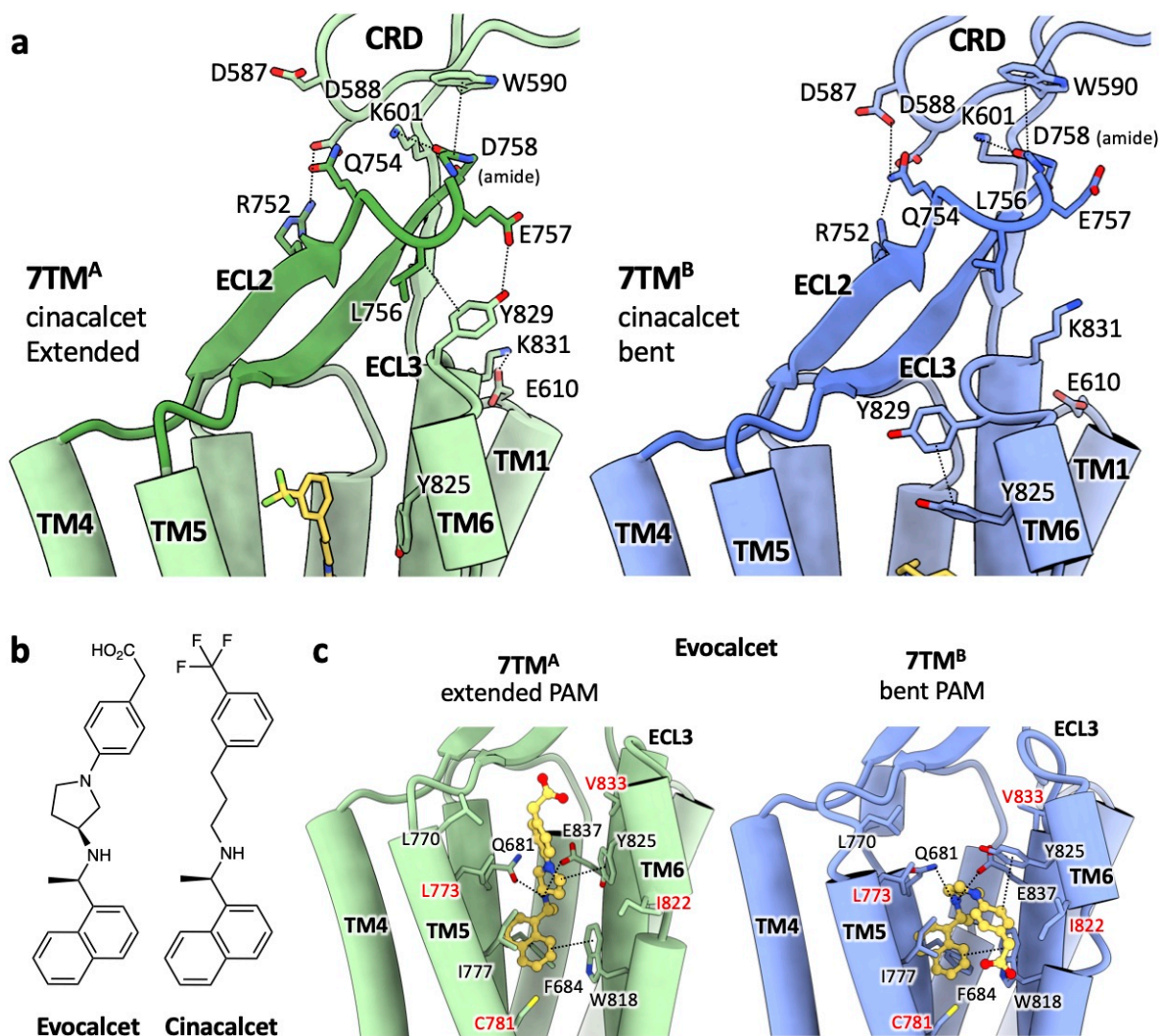
1 **Extended Data Figure 5. a**, ECD from inactive-state CaSR cryo-EM structure with the loop  
 2 tethering the opposing LB1 colored in red. **b**, ECD from inactive-state mGlu5 cryo-EM structure<sup>8</sup>

1 (PDB: 6N51). **c**, inactive-state CaSR ECD crystal structure<sup>6</sup> (PDB: 5K5T). **d**, 7TMs from inactive-  
2 state CaSR cryo-EM structure (grey) superposed onto inactive CaSR ECD crystal structure based  
3 on CRD alignment. **e**, Comparison of inactive 7TMs orientations between CaSR and mGlu5. **f**,  
4 Active-state CaSR cryo-EM structure aligned with the active CaSR ECD crystal structure<sup>6</sup> (grey,  
5 PDB: 5K5S) illustrating the difference in CRD orientations. **g**, Elongated densities observed at the  
6 TM6-TM6 interface in cryo-EM maps of active-state CaSR shown with TM6 residues forming the  
7 cholesterol-binding CARC motif. **h**, Sequence alignment logo showing the conservation of CARC  
8 motif residues among family C GPCRs (generated using alignment from GPCRdb<sup>42</sup> with  
9 WebLogo<sup>43</sup>). **i**, Comparison of Ca<sup>2+</sup> sites in active-state cryo-EM structures with Ca<sup>2+</sup> sites in  
10 active CaSR ECD crystal structure (PDB: 5K5S)<sup>6</sup>. **j**, Alignment of the closed VFT protomer (dark  
11 blue) observed in our inactive-state CaSR structure with either the inactive open protomer (left,  
12 dark green) or the active closed protomer (right, light green). **k**, The tube shaped density observed  
13 in closed inactive CaSR VFT with L-Trp docked in. **l**, Crystal structure of open-closed mGlu1  
14 VFTs<sup>13</sup> (PDB: 1EWV).

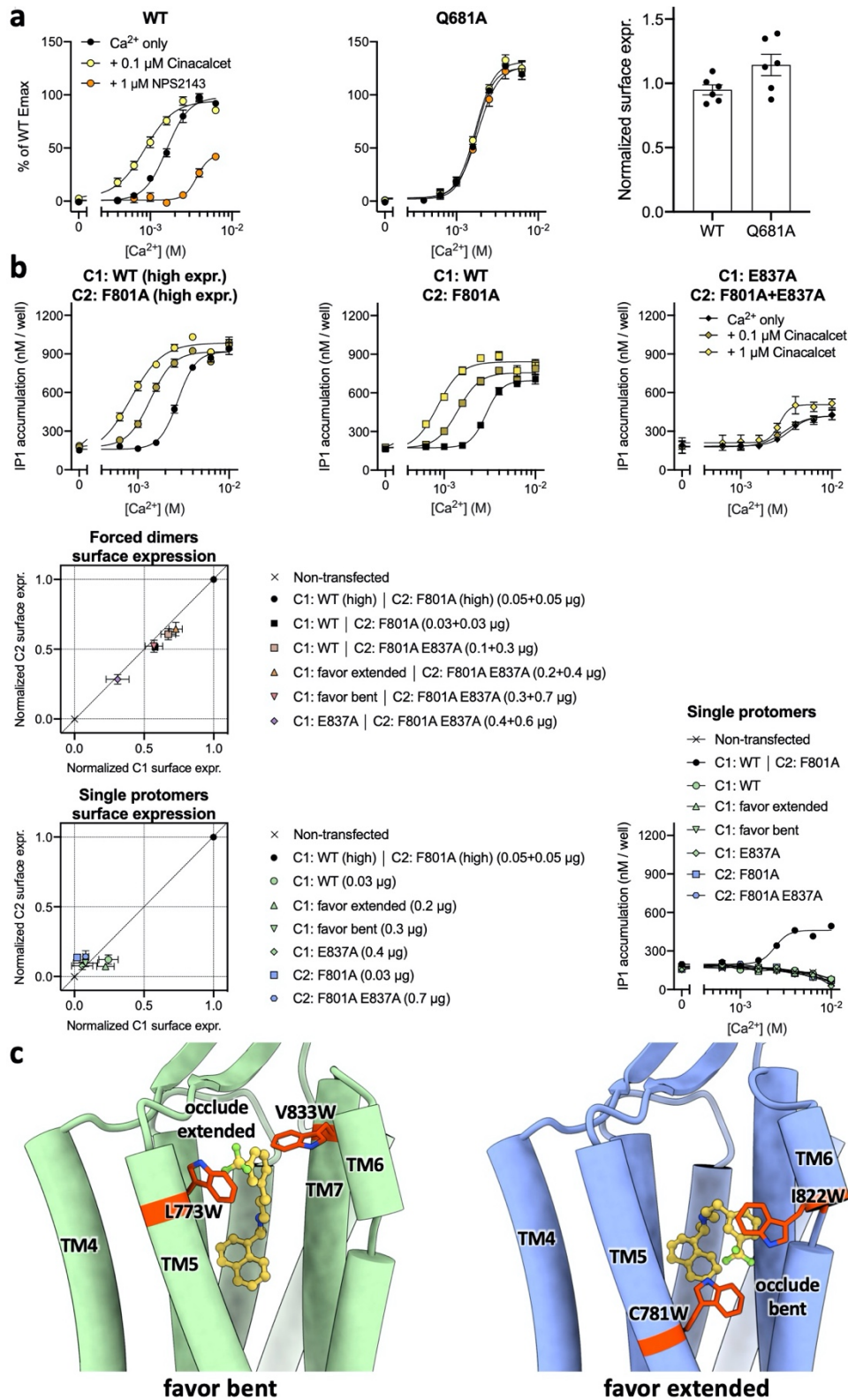


1 **Extended Data Figure 6. PAM and NAM models and TM6-TM6 interfaces in cryo-EM**  
 2 **densities. a**, Etelcalcetide model in cryo-EM density. **b**, Active-state CaSR TM6-TM6 interface  
 3 model in cryo-EM density (shown here is CaSR-cinacalcet. The TM6-TM6 interface of CaSR-  
 4 evocalcet-etelcalcetide is highly similar). **c**, Cinacalcet models in cryo-EM densities. **d**, Evocalcet  
 5 models in cryo-EM densities. **e**, NAM model in cryo-EM density for the CaSR-NAM-Ca<sup>2+</sup>-Trp  
 6 complex. **f**, CaSR-NAM-Ca<sup>2+</sup>-Trp complex TM6-TM6 interface model in cryo-EM density. **g**,  
 7 Inactive-state NAM binding pocket. **h**, Inactive-state NAM model in cryo-EM density.





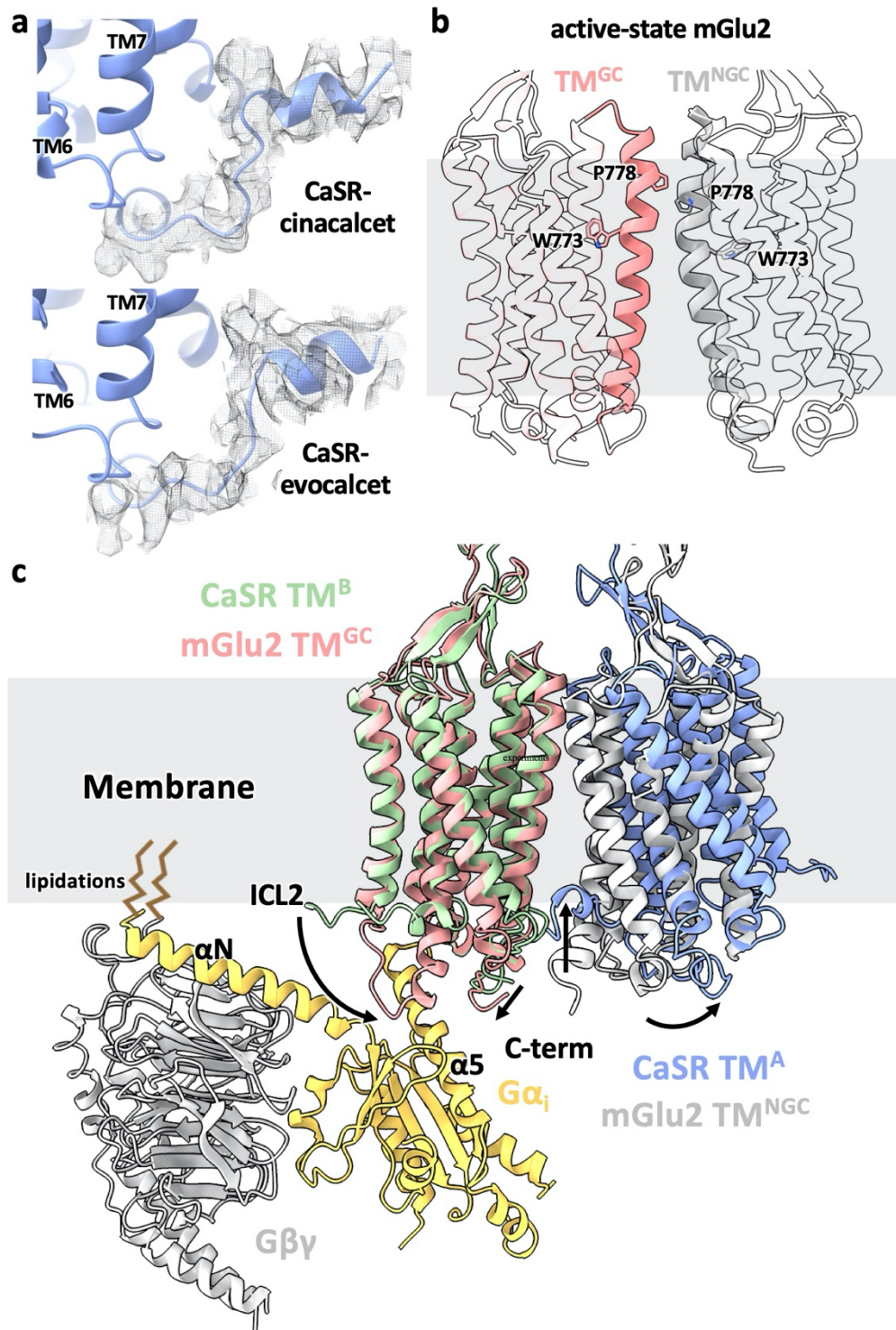
**Extended Data Figure 7.** **a**, Interaction network in the CRD-ECL2-ECL3 region of evocalcet-bound active-state CaSR. **b**, Chemical structures of evocalcet and cinacalcet. **c**, Structure of active-state CaSR 7TMs complexed with evocalcet. Similar to cinacalcet (Fig. 3a), evocalcet adopts an extended conformation in 7TM<sup>A</sup> (green) and a bent conformation in 7TM<sup>B</sup> (blue), making distinct interactions with the two protomers.



1 **Extended Data Figure 8. a,** Ca<sup>2+</sup> response curves (left and middle panels) of the wild-type or

2 Q681<sup>3.33</sup>A mutant CaSR expressed at similar levels (plasma membrane expression levels shown

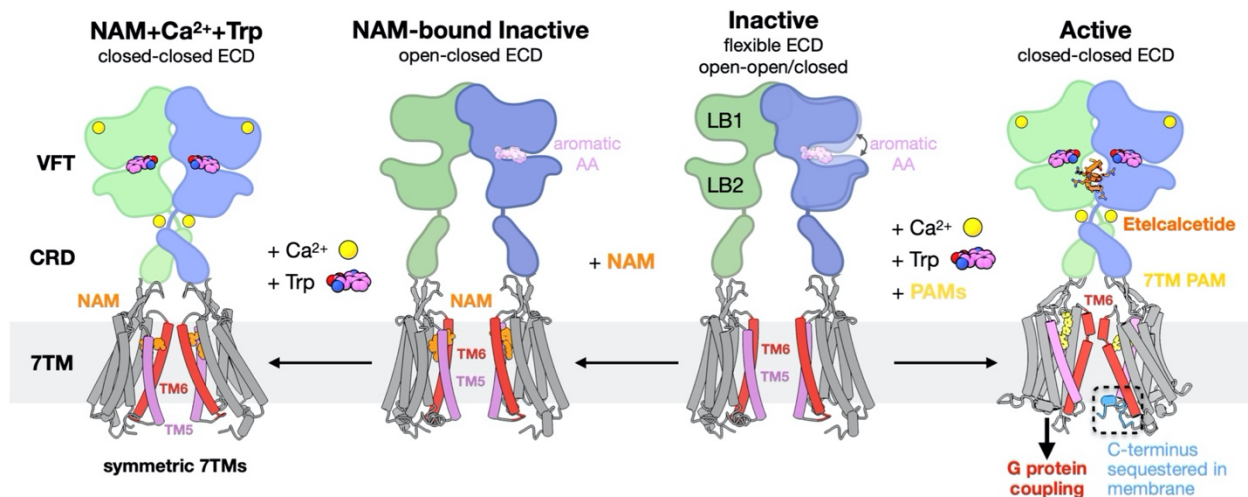
1 on the right panel) in HEK293 cells in the absence or presence of the PAM cinacalcet or NAM  
2 NPS-2143 as monitored by IP<sub>1</sub> accumulation assays. Data represent mean  $\pm$  s.e.m. from six  
3 independent experiments each performed in duplicate. **b**, Top three panels depict results from IP<sub>1</sub>  
4 accumulation assays monitoring the Ca<sup>2+</sup> responses of the CaSR heterodimer without or with the  
5 PAM-binding deficient mutant E837A in both protomers. Middle and bottom left panels show  
6 results from cell surface ELISA assays verifying the different C1 and C2 construct combinations  
7 yield similar expression levels of CaSR heterodimer at the plasma membrane. Bottom right panel  
8 shows the transfection with only one protomer containing either a C1 or C2 tail results in no IP<sub>1</sub>  
9 accumulation signals in response to stimulation with Ca<sup>2+</sup>. Functional IP<sub>1</sub> data represent mean  $\pm$   
10 s.e.m. from 5 independent experiments (top row) or 3 independent experiments (3rd row) each  
11 performed in duplicate, whereas cell surface ELISA data represent mean  $\pm$  s.e.m. from 3  
12 independent experiments performed in triplicate. **c**, Structural illustrations of how the introduced  
13 mutations would occlude extended or bent PAM conformations.



1 **Extended Data Figure 9. a**, The ordered C-terminus from the 7TM with a bent PAM (7TM<sup>B</sup>)  
 2 shown in cryo-EM densities with unsharpened maps. **b**, Asymmetric 7TMs in the active-state  
 3 mGlu2 alone structure (accompanying manuscript). TM6 are shown as solid cartoon with

1 representative residues shown as sticks to highlight the asymmetry. **c**, Superposition of the G  
2 protein-coupling 7TM (7TM<sup>GC</sup>) from mGlu2-G<sub>i</sub> complex structure (accompanying manuscript)  
3 onto the active-state CaSR 7TM with a straight PAM (7TM<sup>A</sup>) showing that the G protein would  
4 fit well on the membrane plane and the tilt of CaSR 7TM<sup>B</sup> leads to the sequestration of its C-  
5 terminus in the membrane. The comparison between mGlu 7TM<sup>GC</sup> and CaSR 7TM<sup>A</sup> illustrates  
6 that the receptor likely would couple to G proteins through downward extensions of both ICL2  
7 and C-terminus.





**Extended Data Figure 10. Schematic of CaSR activation mechanism.** In the inactive state, CaSR is relatively flexible and the 7TMs are separated facing each other at the TM5-TM6 plane. The VFTs adopt inactive open-open/closed conformations. The open-closed conformation can be stabilized by aromatic amino acids (AAs) or their derivatives, thus priming the receptor for activation. NAM binds at both 7TMs with the same conformation and locks the TM6 toggle switch in an inactive conformation. Under high Ca<sup>2+</sup> and high Trp conditions, the ECD adopts a closed-closed active conformation, while the presence of the NAM prevents the 7TMs from adopting the active asymmetric configuration. Upon activation by high Ca<sup>2+</sup> concentration, the VFTs adopt an active closed-closed conformation, which is stabilized by L-Trp bound at the cleft of each VFT and the ECD PAM etelcalcetide further stabilizes the interface between LB2 of the closed-closed VFTs. Closure of the VFTs leads to rearrangement of the CRDs, bringing the 7TMs together to form an asymmetric TM6-TM6 interface. The asymmetric configuration is stabilized by 7TM PAMs adopting distinct poses. The 7TM with a bent PAM is more tilted than the opposing 7TM with its C-terminus sequestered in the membrane, and likely unable to couple to G protein.

1 **Extended Data Table 1. Cryo-EM data collection, refinement and validation statistics.**

	CaSR+evocalcet +etelcalcetide	CaSR+cinacalcet	CaSR+NPS2143	CaSR+NPS2143 +Ca <sup>2+</sup> +L-Trp
<b>Data collection and processing</b>				
Magnification	81,000	81,000	81,000	105,000
Voltage (kV)	300	300	300	300
Electron exposure (e <sup>-</sup> /Å <sup>2</sup> )	64.9	64.9	64.9	60.9
Defocus range (μm)	-0.7~-1.5	-0.7~-1.5	-0.7~-1.5	-0.8~-1.8
Pixel size (Å)	1.11	1.11	1.11	0.8677
Symmetry imposed	C1	C1	C1	C1 (ECD) C2 (TMD)
Initial particle images (no.)	5,181,204	2,718,437	3,825,262	1,592,332
Final particle images (no.)	482,939	253,836	329,093	131,620
Map resolution (Å)	2.5	2.8	4.1	3.2
FSC threshold	(0.143)	(0.143)	(0.143)	(0.143)
<b>Refinement</b>				
Initial model used (PDB code)	5K5S, 6N51	5K5S, 6N51	5K5T, 6N52	5K5S, 6N51
Model composition				
Non-hydrogen atoms	13298	13084	10997	13092
Protein residues	1627	1631	1562	1624
Ligands	EVO: 2 etelcalcetide: 2 TRP: 2 Ca <sup>2+</sup> : 4 PO <sub>4</sub> <sup>3-</sup> : 2 NAG: 15	CIN: 2 TRP: 2 Ca <sup>2+</sup> : 4 PO <sub>4</sub> <sup>3-</sup> : 2 NAG: 15	NPS: 2 PO <sub>4</sub> <sup>3-</sup> : 2 NAG: 7	NPS: 2 TRP: 2 Ca <sup>2+</sup> : 4 PO <sub>4</sub> <sup>3-</sup> : 2 NAG: 11
B factors (Å <sup>2</sup> )				
Protein	57.4	56.2	69.3	21.2
Ligands	Evocalcet <sub>bent</sub> : 94.0 Evocalcet <sub>extd</sub> : 93.0 Etelcalcetide: 52.2 TRP: 31.1 Ca <sup>2+</sup> (site 1): 42.0 Ca <sup>2+</sup> (site 2): 66.9 PO <sub>4</sub> <sup>3-</sup> : 27.0 NAG: 54.9	Cinacalcet <sub>bent</sub> : 82.0 Cinacalcet <sub>extd</sub> : 83.1 TRP: 32.7 Ca <sup>2+</sup> (site 1): 41.9 Ca <sup>2+</sup> (site 2): 75.8 PO <sub>4</sub> <sup>3-</sup> : 35.4 NAG: 55.8	NPS-2143: 137.8 PO <sub>4</sub> <sup>3-</sup> : 32.6 NAG: 76.9	NPS-2143: 31.2 Ca <sup>2+</sup> (site 1): 22.2 Ca <sup>2+</sup> (site 2): 49.8 PO <sub>4</sub> <sup>3-</sup> : 3.8 NAG: 23.2 TRP: 1.9
R.m.s. deviations				
Bond lengths (Å)	0.006	0.008	0.009	0.006
Bond angles (°)	0.935	1.008	1.085	0.931
Validation				
MolProbity score	1.18	1.39	1.45	1.24
Clashscore	2.25	2.56	2.66	1.94
Poor rotamers (%)	0.93	0.00	0.12	0.00
CaBLAM outliers (%)	1.69	1.88	2.94	2.83
EMRinger score	3.70	4.26	2.90	3.66
Ramachandran plot				
Favored (%)	96.95	94.98	93.98	95.89
Allowed (%)	3.05	5.02	6.02	4.11
Outliers (%)	0.00	0.00	0.00	0.00

**Supplementary Video 1. Inactive-state CaSR 3D variability analysis component 1.** Particles of inactive-state CaSR were subjected to 3D variability analysis. This video illustrates the motions corresponding to the first principal component revealed by the analysis.

**Supplementary Video 2. Inactive-state CaSR 3D variability analysis component 2.** Particles of inactive-state CaSR were subjected to 3D variability analysis. This video illustrates the motions corresponding to the second principal component revealed by the analysis.

**Supplementary Video 3. Inactive-state CaSR 3D variability analysis component 3.** Particles of inactive-state CaSR were subjected to 3D variability analysis. This video illustrates the motions corresponding to the third principal component revealed by the analysis.

**Supplementary Video 4. Active-state CaSR 3D variability analysis component 1.** Particles of active-state CaSR complexed with etelcalcetide and evocalcet were subjected to 3D variability analysis. This video illustrates the motions corresponding to the first principal component revealed by the analysis.

**Supplementary Video 5. Active-state CaSR 3D variability analysis component 2.** Particles of active-state CaSR complexed with etelcalcetide and evocalcet were subjected to 3D variability analysis. This video illustrates the motions corresponding to the second principal component revealed by the analysis.

**Supplementary Video 6. Active-state CaSR 3D variability analysis component 3.** Particles of active-state CaSR complexed with etelcalcetide and evocalcet were subjected to 3D variability analysis. This video illustrates the motions corresponding to the third principal component revealed by the analysis.